

# CAN RT MODELS + DUST EMISSION SEDS UNLOCK THE SECRETS OF DUST IN ELLIPTICAL GALAXIES?



**N.K. Agius<sup>1</sup>**

**G. Natale<sup>1</sup>, C.C. Popescu<sup>1</sup>**

**A.E. Sansom<sup>1</sup>, R. Tuffs<sup>2</sup>**

<sup>1</sup>Jeremiah Horrocks Institute,  
University of Central Lancashire,

<sup>2</sup>Max-Planck-Institut Für Kernphysik

GAMA



## OVERVIEW

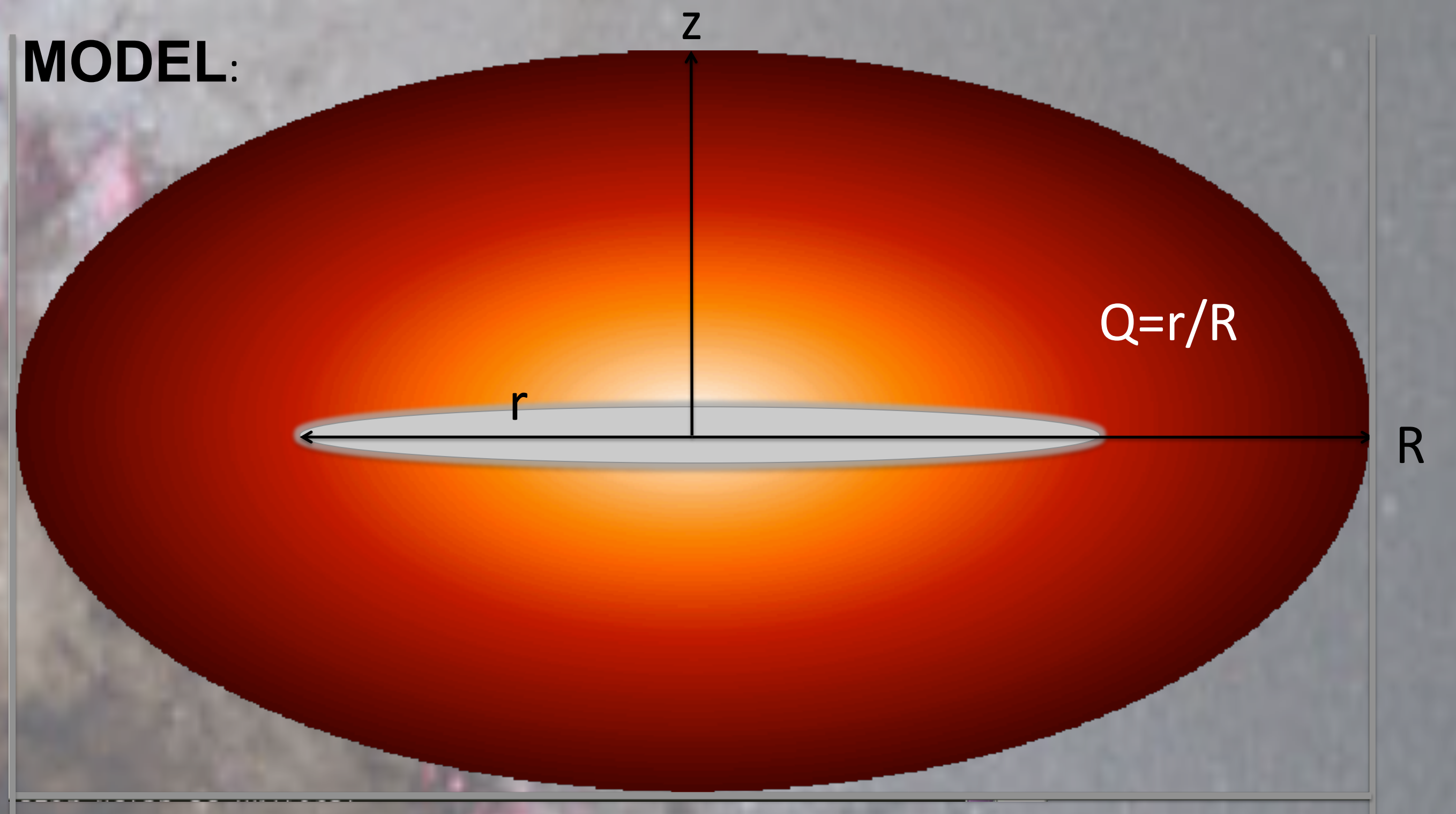
Although dust disks are known to form part of spiral galaxies, the geometrical distribution of dust in elliptical galaxies has yet to be well determined. This is because the Far-Infrared dust continuum emission in ellipticals is relatively faint (Kaneda *et al.*, 2008). However the Herschel Space Observatory has provided new, higher resolution data which has improved our ability to detect dust emission in these systems.

In particular, it is unclear whether the dust is in a rotationally supported interstellar medium within a disk, or whether the dust is distributed throughout a hot interstellar medium. Using a selection of UV-bright elliptical galaxies from Agius *et al.* (2013; A13), all of which contain significant dust masses, we fit dust emission SED templates to a combination of WISE MIR, Herschel FIR and sub-mm data. We applied the same SED fitting technique to a control set of Virgo ellipticals with Herschel data, presented in di Serego Aligheri *et al.* (2013).

We performed radiative transfer (RT) calculations for a spheroid with a range of Sérsic indices containing dust assembled in a disk, based on models in Popescu *et al.* (2011). We compared the radiation field energy density inferred from the SED fits with those predicted for the RT models. This procedure is performed when the solution is in the optically thin regime.

We are using the above analysis to infer characteristic radii for the distribution of dust in these galaxies, which will help to obtain insights about the geometrical distribution and the origin of dust.

## MODEL:

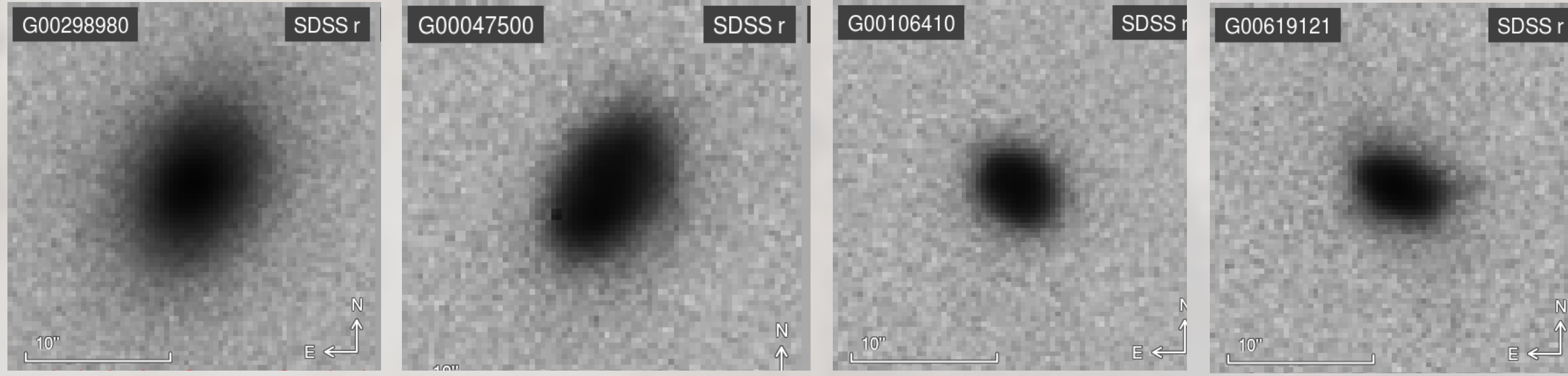


Optical Properties of Dust Grains:  
Weingartner & Draine (2001)

Parameters of the Model:  
 $\tau_B = 0.1, 0.3, 0.5, 1.0, 2.0, 4.0, 8.0$   
 $n = 1.0, 2.0, 4.0, 8.0$   
↳ constrained by observations

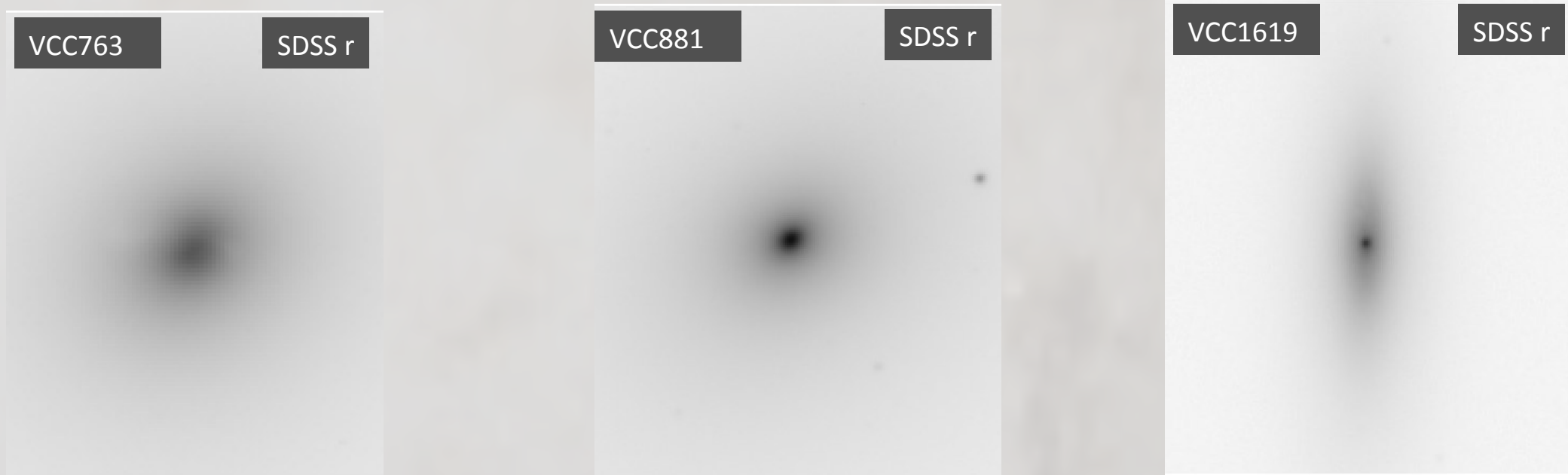
$$U_{\text{rad,mod,scaled}} = U_{\text{rad,mod}} \times \frac{L_{\text{gal}}/R_{\text{eff,gal}}^2}{L_{\text{mod}}/R_{\text{eff,mod}}^2}$$

## Elliptical Galaxies



### A13 ELLIPTICALS

$M_r \sim -20$  mags  
 $M_d \sim 10^7 M_\odot$   
 $L_{\text{IR}} \sim 10^{43}$  ergs s<sup>-1</sup>



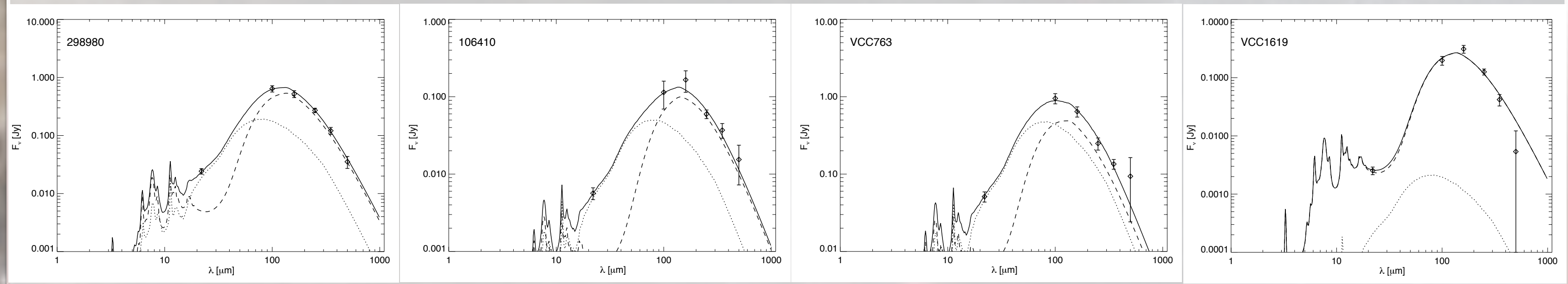
### VIRGO CLUSTER ELLIPTICALS

$M_r \sim -21.5$  mags  
 $M_d \sim 10^5 M_\odot$   
 $L_{\text{IR}} \sim 10^{42}$  ergs s<sup>-1</sup>

## SED Fits: Diffuse + Photo-Dissociation Region Dust Emission Templates

Natale *et al.* (2010), Fischera & Dopita (2008)

Four Components: UV emission from young stars + 3 blackbody curves



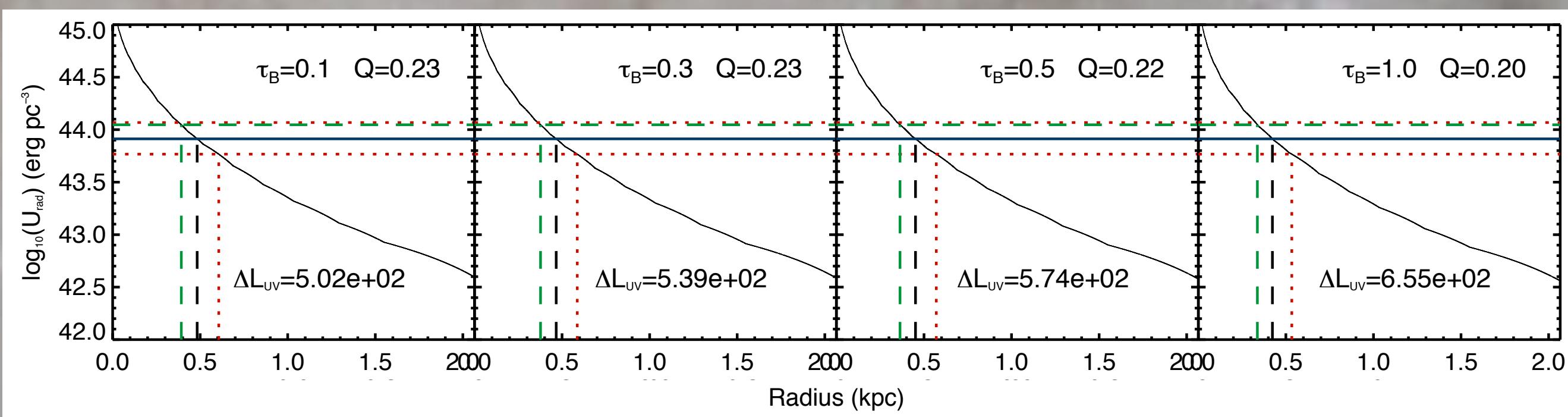
### Outputs:

$X_{\text{UV}}$  = amplitude of the UV radiation field energy density  
 $X_{\text{col}}$  = amplitude of the optical part of the radiation field divided by  $X_{\text{UV}}$   
 $M_d$  = derived mass of galaxy's dust distribution

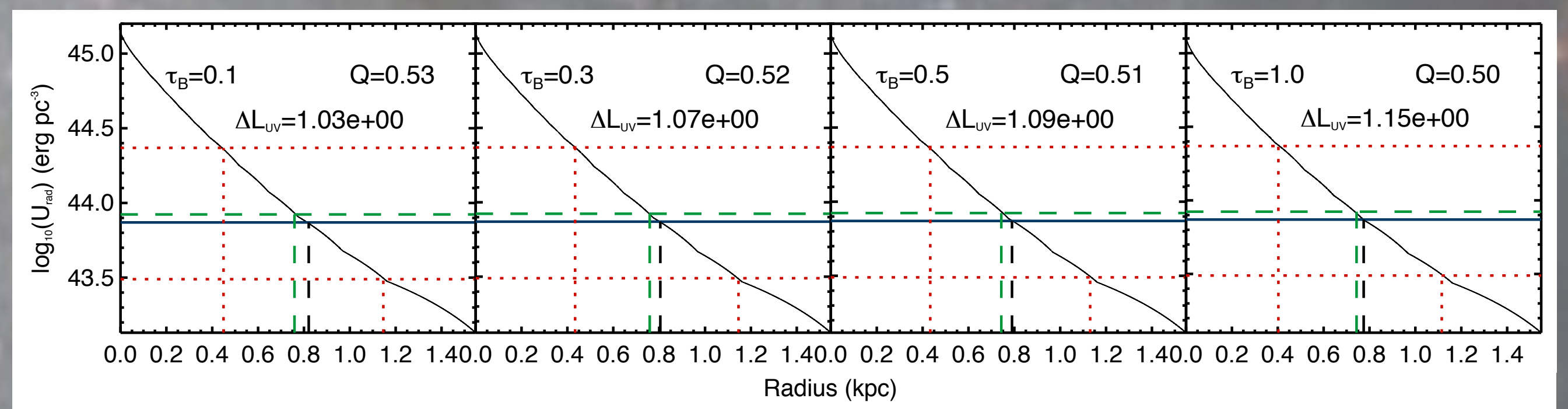
$$U_{\text{rad,gal}} = \chi_{\text{col}} \times \chi_{\text{UV}} \times \text{ISRF}_{\text{Mathis}}$$

ISRF<sub>Mathis</sub> = interstellar radiation field as defined by Mathis *et al.* (1983)

## A13 298980



## VIRGO VCC1619



The scaled model energy density ( $U_{\text{rad,mod}}$ ) distributions are shown for a galaxy from the A13 sample (left) and the Virgo sample (right) as a function of radius. Black dashed lines show the radius where the  $U_{\text{rad,mod}}$  intersect with the estimated galaxy energy density ( $U_{\text{rad,gal}}$ ), with upper and lower limits represented by red dotted lines. From left to right,  $U_{\text{rad,mod}}$  is calculated with increasing face-on B-band opacity ( $\tau_B$ ).  $Q$  represents the fraction of the galaxy's effective radius which is occupied by the dust disk.

## RESULTS

1. Virgo ellipticals are found to have dust disk sizes filling 50-100% of the effective radii of their spheroidal component.
2. Virgo elliptical results are consistent with the dust distribution being optically thin.
3. A13 ellipticals are not consistent with being optically thin.
4. A13 ellipticals need an optically thick solution to appreciate their dust distributions.
5. These results are consistent with A13 ellipticals forming part of the elliptical population which has not yet finished evolving (see Agius *et al.*, 2013).

## REFERENCES

- Agius *et al.*, 2013, MNRAS, 431, 1929  
di Serego Alighieri *et al.*, 2013, A&A, 552, A8  
Fischera & Dopita, 2008, ApJS, 176, 164  
Kaneda *et al.*, 2008, PASJ, 60, 467  
Mathis *et al.*, 1983, A&A, 128, 212  
Natale *et al.*, 2010, ApJ, 725, 955  
Popescu *et al.*, 2011, A&A, 527, 109  
Weingartner & Draine, 2001, ApJ, 548, 296

# Are U/LIRGS evolving into Elliptical Galaxies?

## Probing the Build-up of Nuclear Stellar Cusps

S. Haan, L. Armus, J. A. Surace, V. Charmandaris, A.S. Evans, D.B. Sanders, and the GOALS team

ASTRONOMY & SPACE SCIENCE  
www.csiro.au



Nuclear stellar cusps are defined as central excess light component in the stellar light profiles of galaxies and are suggested to be stellar relics of intense compact starbursts in the central 100–500 pc region of gas-rich major mergers. Here we probe for the first time the build-up of nuclear cusps during the actual starburst phase for a complete sample of Luminous Infrared Galaxy systems and compare their nuclear properties to elliptical galaxies as tracer of their evolutionary linkage.

Evidence for a nuclear cusp build-up has been found so far in a significant fraction of early-type galaxies and merger remnants (e.g; Lauer et al. 1995; Faber et al. 1997; Rothberg & Joseph 2004; Cote et al. 2007; Hopkins et al. 2008; Kormendy et al. 2009). Follow-up studies have shown a strong dependence on the optical luminosity of the host galaxy, leading to a dichotomy between core (flat profile towards the center) and cusp galaxies (characterized by a steep inner slope), with core galaxies dominating at the highest luminosities and cusp galaxies at the lowest. However, until recently there has been little observational evidence on the build-up of these cusps during the actual merger-induced starburst stage. While previous ground-based observations have revealed that a significant fraction of merger remnants seems to exhibit radial profiles similar to elliptical galaxies based on their large-scale appearance, we are now able to link for the first time the stellar light distribution and merger-induced starburst in the central kpc for a large sample of nearby active starburst mergers.

### THE HST GOALS SAMPLE

We have imaged the 85 most luminous U/LIRGs (with  $11.4 < \log[L_{\text{IR}}/L_{\odot}] < 12.5$ ) of the GOALS sample (Armus et al. 2009) in the near-IR (1.6  $\mu\text{m}$ ) using the Hubble Space Telescope (NICMOS/WFC3). Cusp properties are derived via 2-dimensional fitting (GALFIT) of the nuclear stellar light and have been combined with mid-IR diagnostics for AGN/starburst characterization (using Spitzer and Herschel spectroscopy).

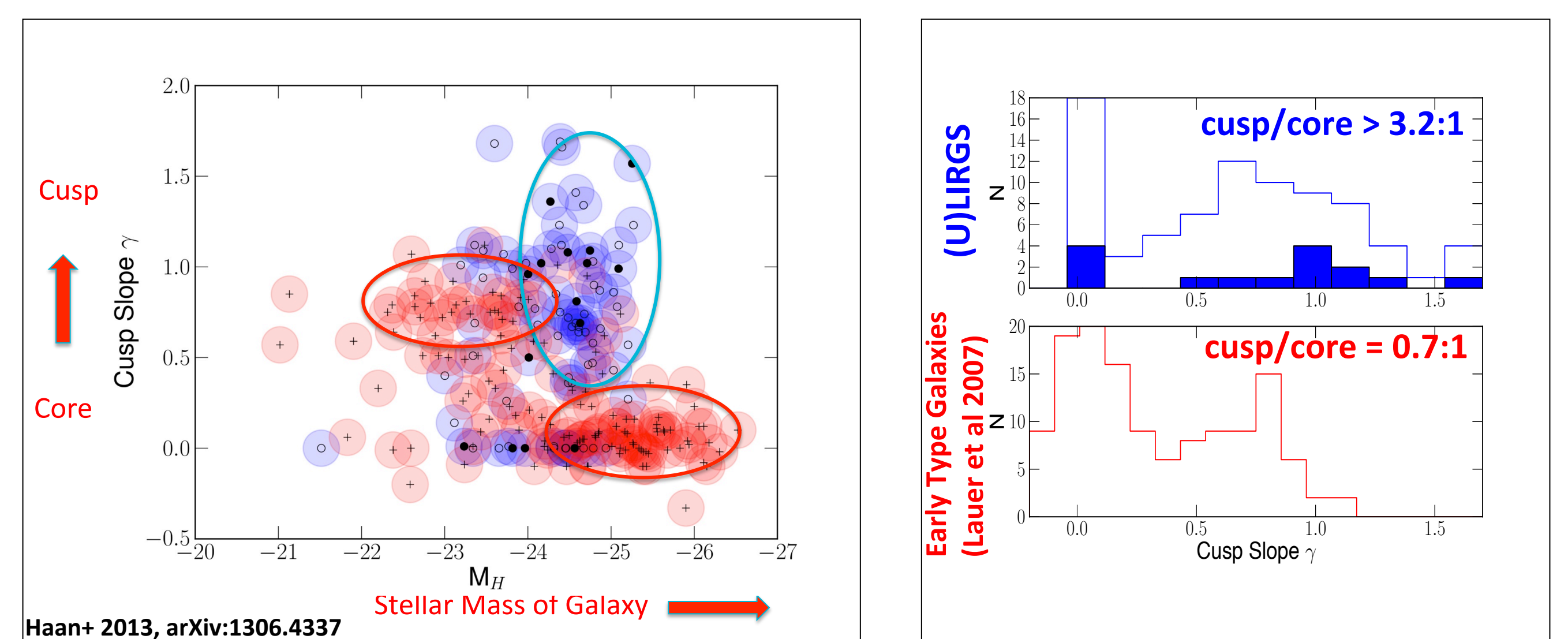


Figure 3: Comparison of cusp and core properties in nearby (U)LIRGs (blue) to those of present day core and cusp dominated ellipticals (red). Left: The Nuker gamma parameter as a function of the absolute H-band magnitude (2MASS) of the host galaxy. Right: Histogram of the Nuker gamma parameter for (U)LIRGs and early type galaxies (sample from Lauer et al. 2007) within the same total luminosity range ( $-25.5 < M_H < -22.5$ ). Late stage mergers are indicated as filled histogram (right panel) and filled circles (left panel).

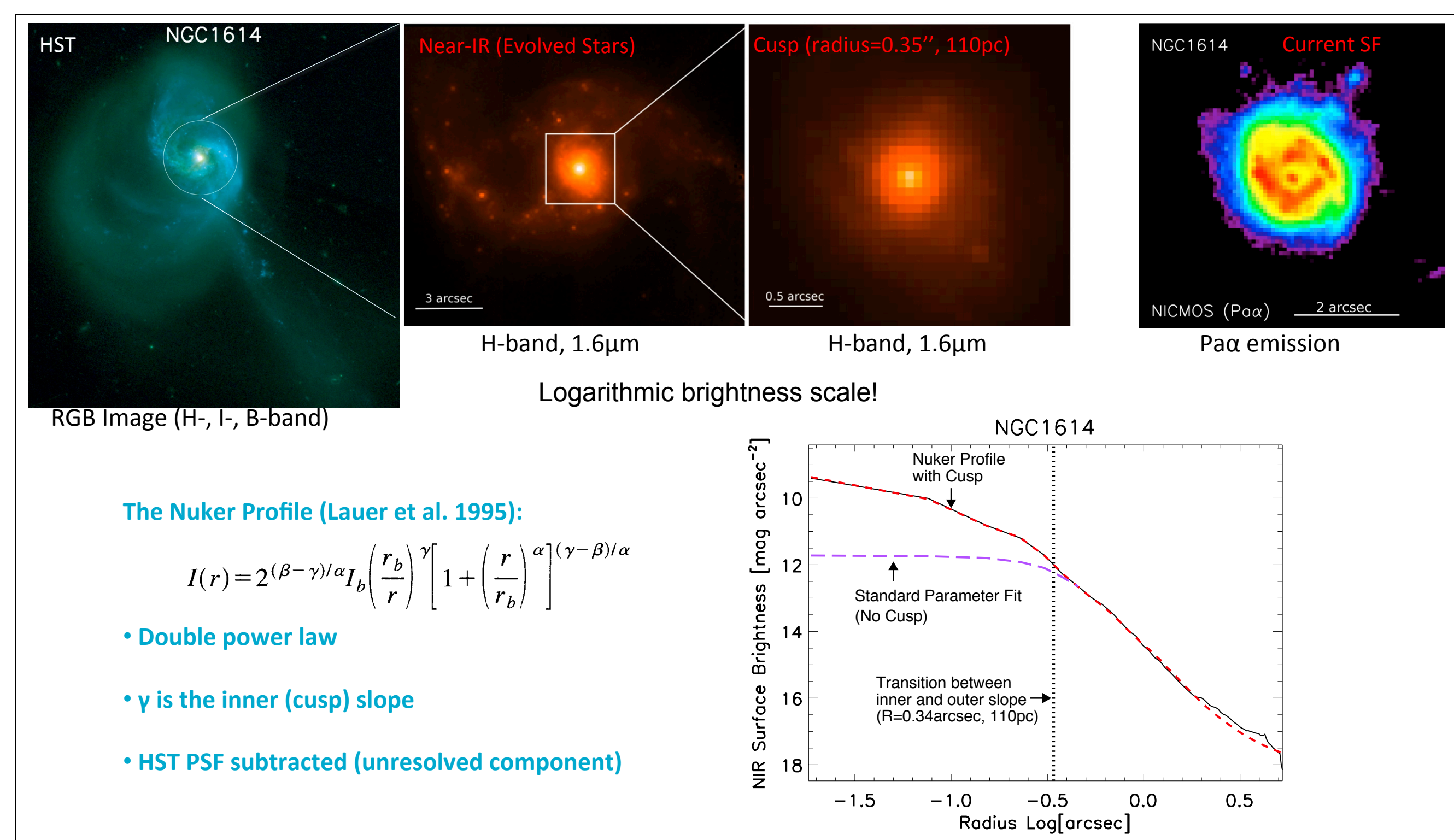


Figure 1: Example of a strong cusp galaxy: The nuclear NIR properties of the late stage merger NGC 1614.

## Results

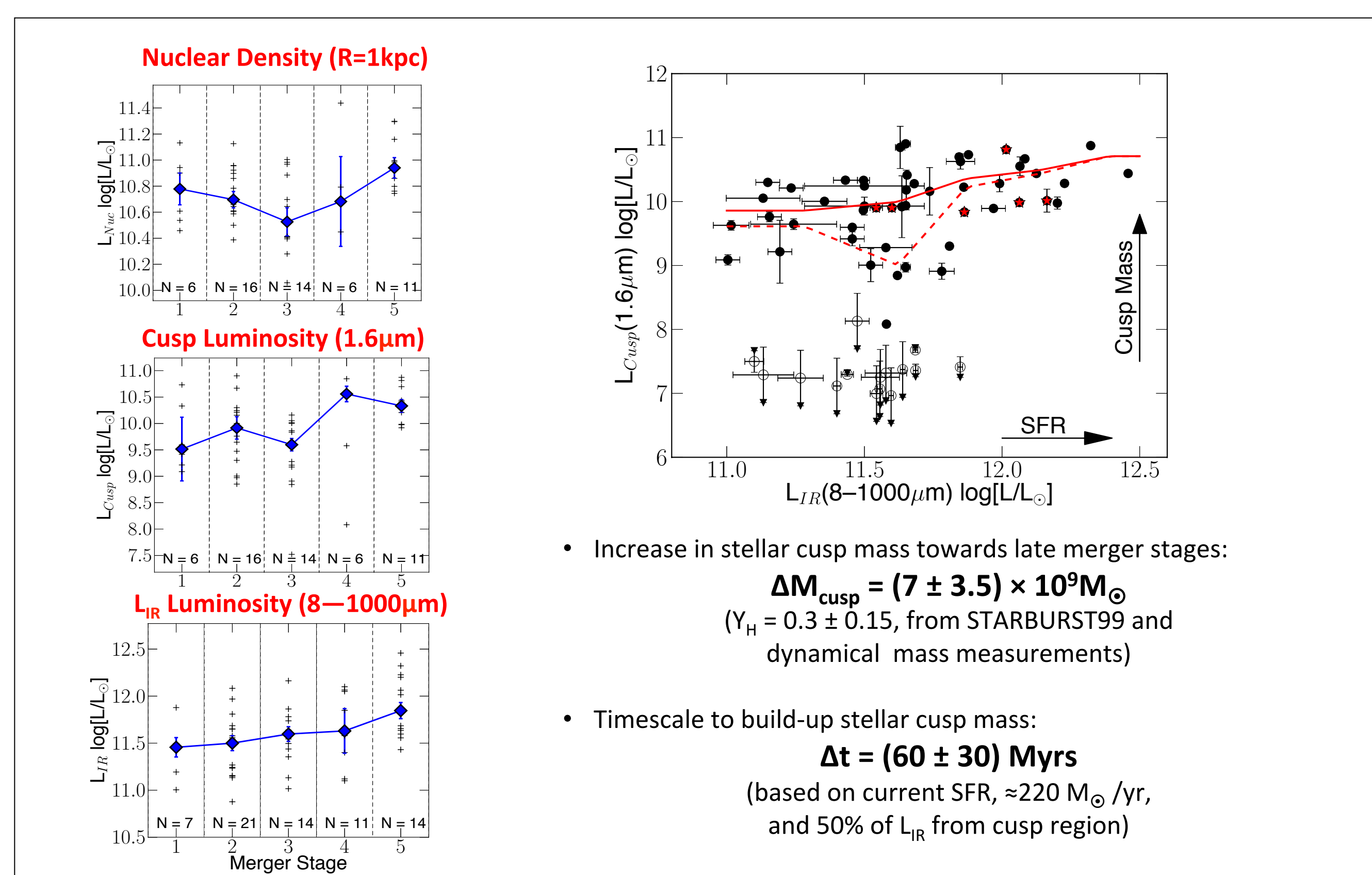
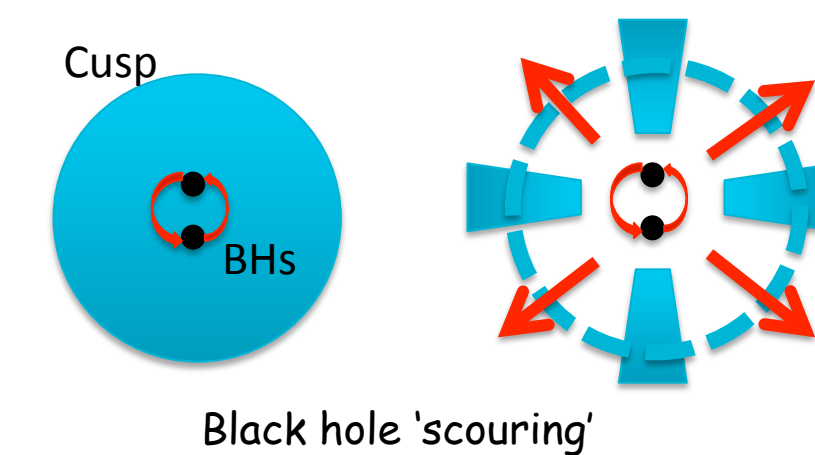


Figure 2: Nuclear NIR properties as function of merger stage (left, 1: early to 5: late stage) and the H-band cusp luminosity as function of the total IR luminosity (right). The contribution from AGN light to the cusp H-band luminosity and to the total IR luminosity is subtracted (Haan et al. 2013). Both results show a significant increase in cusp luminosity.

## Conclusions

- Nuclear stellar cusps are resolved in 76% of (U)LIRGs while the remaining 24% have flat nuclear profiles (core galaxies) with nuclear slopes  $< 0.3$ . The cusp strength and luminosity increase with far-IR luminosity (excluding AGN), confirming models that recent starburst activity is associated with the build-up of stellar cusps. An average increase in cusp luminosity  $\Delta L_{\text{cusp}} \sim 2.5 \times 10^{10} L_{\odot}$  is found as a function of far-IR luminosity and merger stage, which corresponds to a build-up of stellar mass  $\Delta M_{\text{cusp}}$  of  $(7 \pm 3.5) \times 10^9 M_{\odot}$ .
- The nuclear stellar surface brightness profiles of local (U)LIRGs are very different from those of present day's early-type galaxies with comparable masses. Our comparison between (U)LIRGs and a large sample of local elliptical galaxies (within the same host galaxy mass range) reveals (a) a significant larger cusp/core ratio in (U)LIRGs (3.2:1) than in ellipticals (0.7:1), and (b) (U)LIRGs do not follow the cusp to core dependency of ellipticals as a function of host galaxy mass ( $M_H$ - $\gamma$  diagram) and clearly represent a distinct population. Moreover, gas-rich late stage mergers show no indications of a cusp destruction by BH-binary scouring during the coalescence of their nuclei. These results suggest that the progenitors of present day's massive ellipticals must have either expelled most of their gas during a brief episode in cosmic time and destroyed their cusps in subsequent gas-poor re-merger events, or that star formation was quickly shut down before gas could efficiently accumulate in the very center to build up a cusp (e.g. via feedback from supernovae, hot stars, and AGN due to higher gas fractions at high-z).

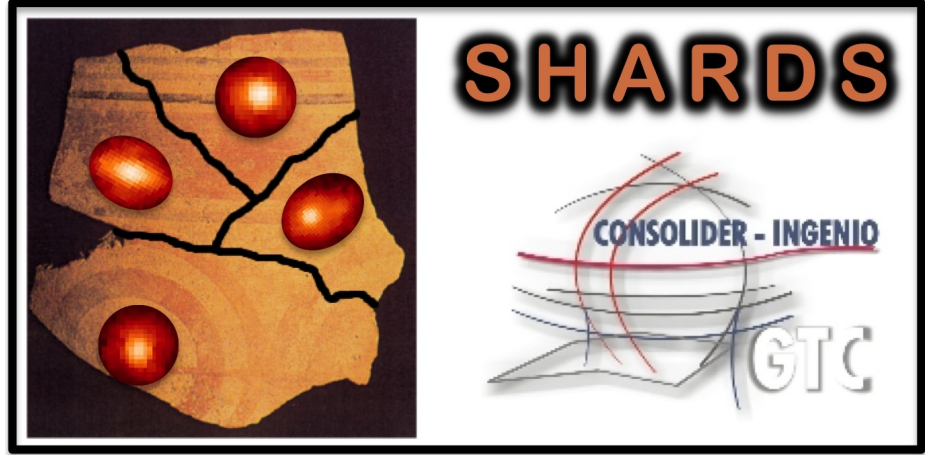


# DECONSTRUCTING MASSIVE GALAXY FORMATION

Ignacio Ferreras<sup>1a</sup>, Ignacio Trujillo<sup>2</sup>, Esther Marmol-Queralto<sup>3</sup>,  
Pablo Perez-Gonzalez<sup>4</sup>, Antonio Cava<sup>4</sup> & SHARDS team

(1) Mullard Space Science Laboratory, University College London, (2) Instituto de Astrofısica de Canarias, (3) Royal Observatory Edinburgh, (4) Universidad Complutense de Madrid.

<sup>a</sup>E-mail: i.ferreras@ucl.ac.uk



## Abstract

We probe the merging channel of massive galaxies ( $\gtrsim 10^{11}M_{\odot}$ ) at  $z \lesssim 1$  by studying a sample extracted from the deep ( $AB < 26.5$ ) SHARDS dataset, that provides medium band photometry, effectively yielding low-resolution  $R \sim 50$  spectra. By selecting massive galaxies with nearby satellites, we focus on the progenitors of the merging systems that allegedly contribute to the size growth over the past 8 Gyr of cosmic time [5]. A strong correlation is found between the age difference of central and satellite galaxy and mass ratio, so that the 1:100 merger progenitors feature age differences  $\sim 4$  Gyr. A simple argument comparing the mass in centrals and satellites within a “merging timescale” suggests a growth factor between  $z \sim 1$  and 0 of  $\Delta M_{1 \rightarrow 0} / M_{z=1} \sim 2.0 \pm 0.3$ , without any significant evolution in that redshift range.

## 1 THE TWO-PHASE EVOLUTION

Massive galaxies appear to have a formation process involving two phases [6], an early stage of intense, *in-situ* star formation, creating the core of the massive galaxy – i.e. building the compact massive galaxies we see at  $z \gtrsim 1-2$  – followed by a second phase that involves a gradual build-up from mergers (minor/major, wet/dry). The homogeneity of the populations of massive galaxies at  $z \sim 0$  (e.g., [3]) suggests that wet mergers cannot play a significant role at  $z \lesssim 1$ . However, it is not clear whether the main growth channel is in the form of major or minor mergers.

## 3 MODELLING STELLAR POPULATIONS

The medium-band photometric information provides a low-resolution ( $R \sim 50$ ) spectral energy distribution that can be used to compare with a large grid of population synthesis models. We build a large library, comprising  $\sim 5 \times 10^5$  models that include simple stellar populations,  $\tau$ -models, and constant star formation histories. We also include a reddening parameter following a standard extinction law, and add an additional free variable to track the emission lines (Ferreras et al., in preparation). The typical mass-age relation is retrieved in our general sample of SHARDS sources.

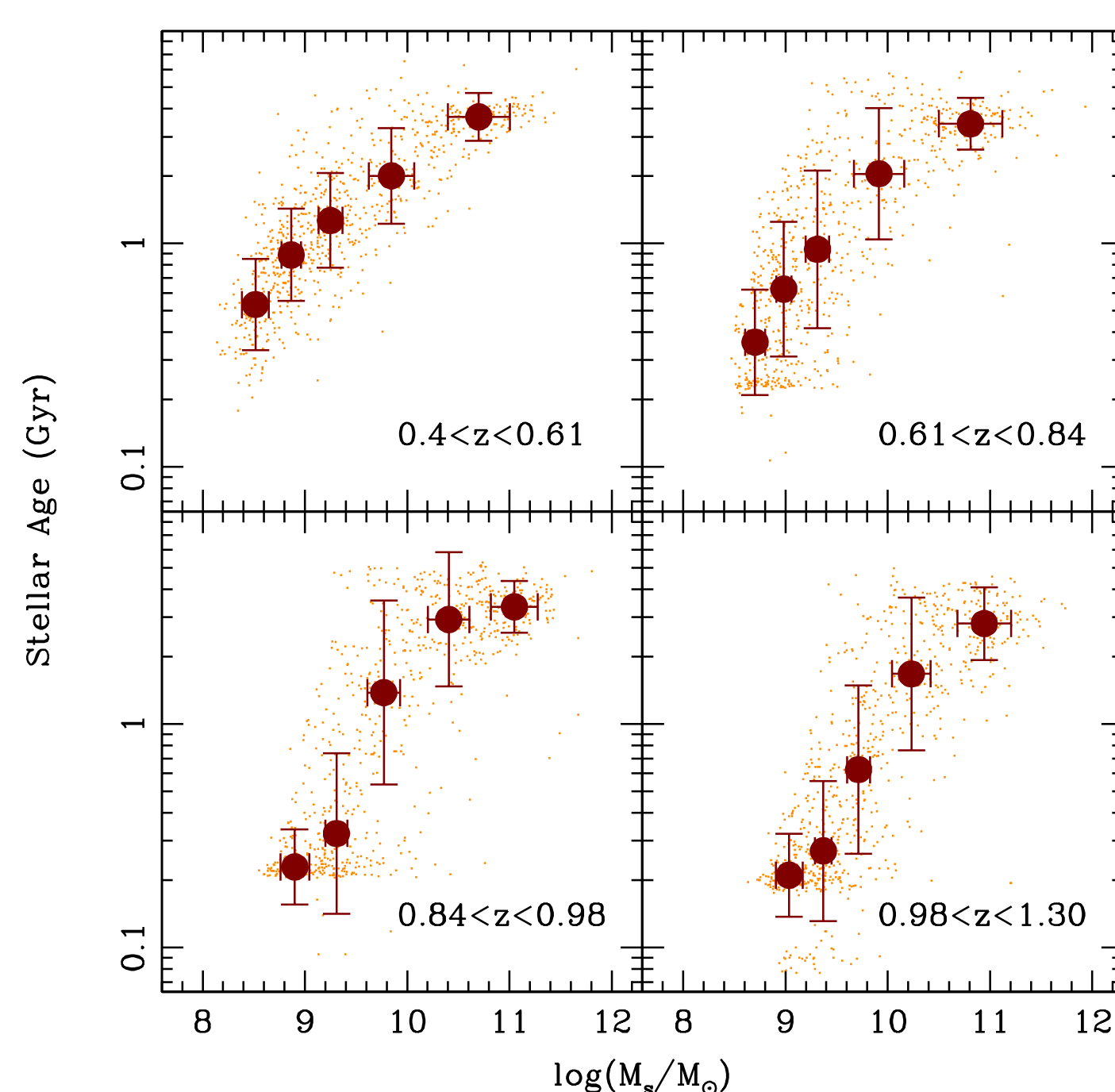


Fig. 2: Mass-age relationship split into quarters in redshift. The red circles give the median and within bins in stellar mass, chosen at a fixed number of galaxies per bin. The errors show the standard deviation within each bin.

## 5 MASS GROWTH

We can also determine the evolution of the mass growth in massive galaxies over the  $z \lesssim 1$  redshift interval. If we take redshift slices as “snapshots” covering a typical merging timescale (e.g. [2]), we can use the mass in centrals and satellites within each snapshot, to determine the amount of stellar mass incorporated into massive galaxies, which should give a good estimate of the growth rate, given that no significant star formation is expected in massive galaxies at low redshift. The figure – shown for three typical merging timescales,  $\Delta T$  – suggest that the growth rate is roughly constant at  $z \lesssim 1$ :

$$\frac{1}{M} \frac{\Delta M}{\Delta t} \sim 0.11 \pm 0.04 \text{ Gyr}^{-1}$$

which translates into a total growth rate between  $z=1$  and 0 of

$$\frac{\Delta M_{z=1 \rightarrow 0}}{M_{z=1}} \sim 2.0 \pm 0.3.$$

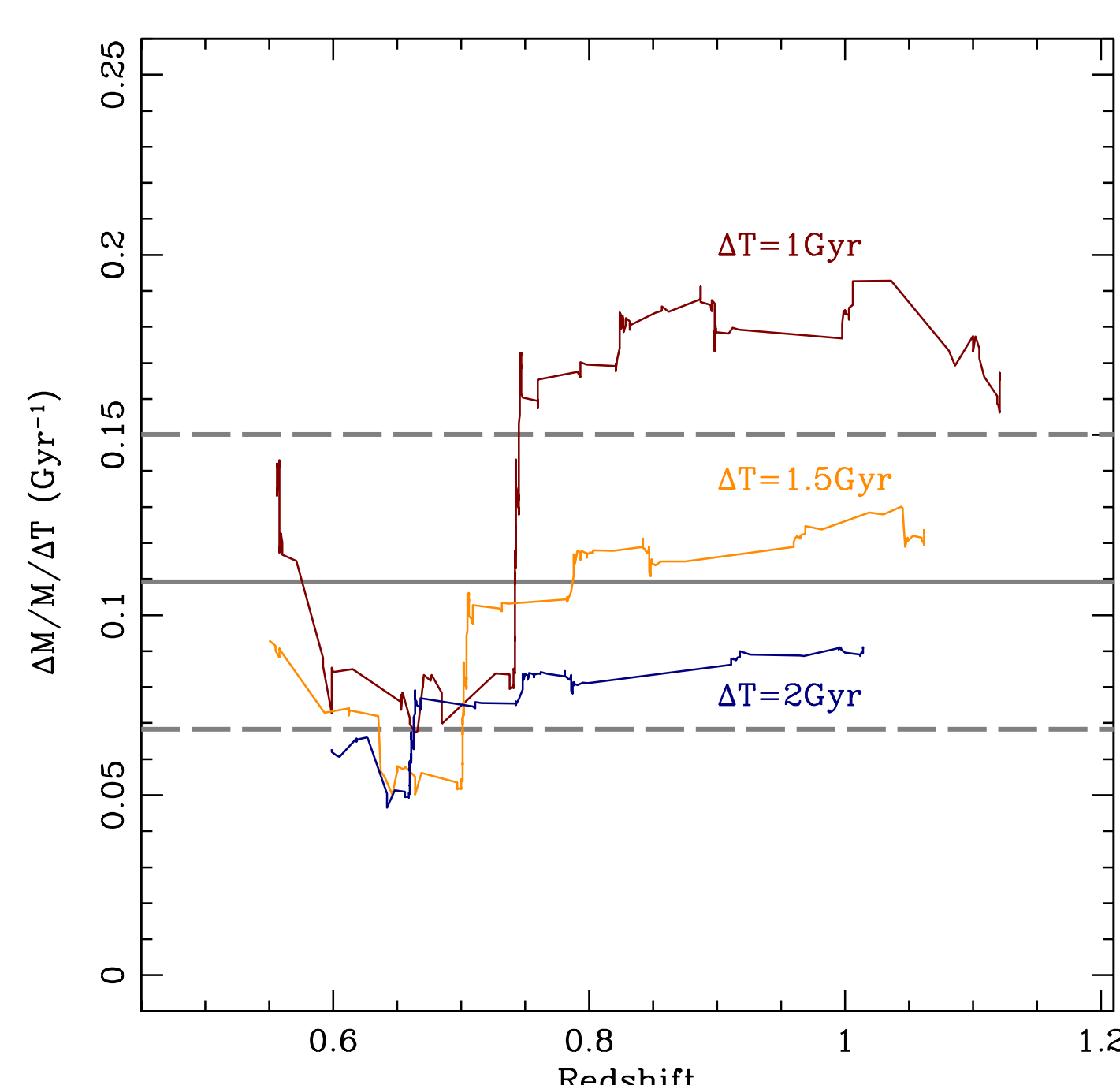


Fig. 4: Stellar mass accretion rate from satellites.

## 2 SHARDS MASSIVE GALAXIES

We assembled a sample of massive galaxies from SHARDS, the Survey for High- $z$  Absorption Red and Dead Sources [7], a deep (26.5 AB) survey towards the GOODS-N field, covering a  $130 \text{ arcmin}^2$  area with 24 medium band ( $\Delta \lambda \sim 170 \text{ \AA}$ ) filters. In this poster, we only use data from the available 16 filters, covering the  $6100-9000 \text{ \AA}$  spectral range. These data allow us to obtain accurate photometric redshifts ( $\Delta z / (1+z) \lesssim 0.01$ ). Out of a preliminary sample of 254 massive galaxies ( $M_s > 10^{11} M_{\odot}$ ), we search for satellites within a projected distance of  $\Delta R < 100 \text{ kpc}$  and at the same redshift – within uncertainties. Note from the figure that out to  $z < 1.3$ , our sample is complete down to a mass ratio of 1:10, and possibly down to 1:100 if we consider that low mass galaxies are dominated by young stellar

populations.

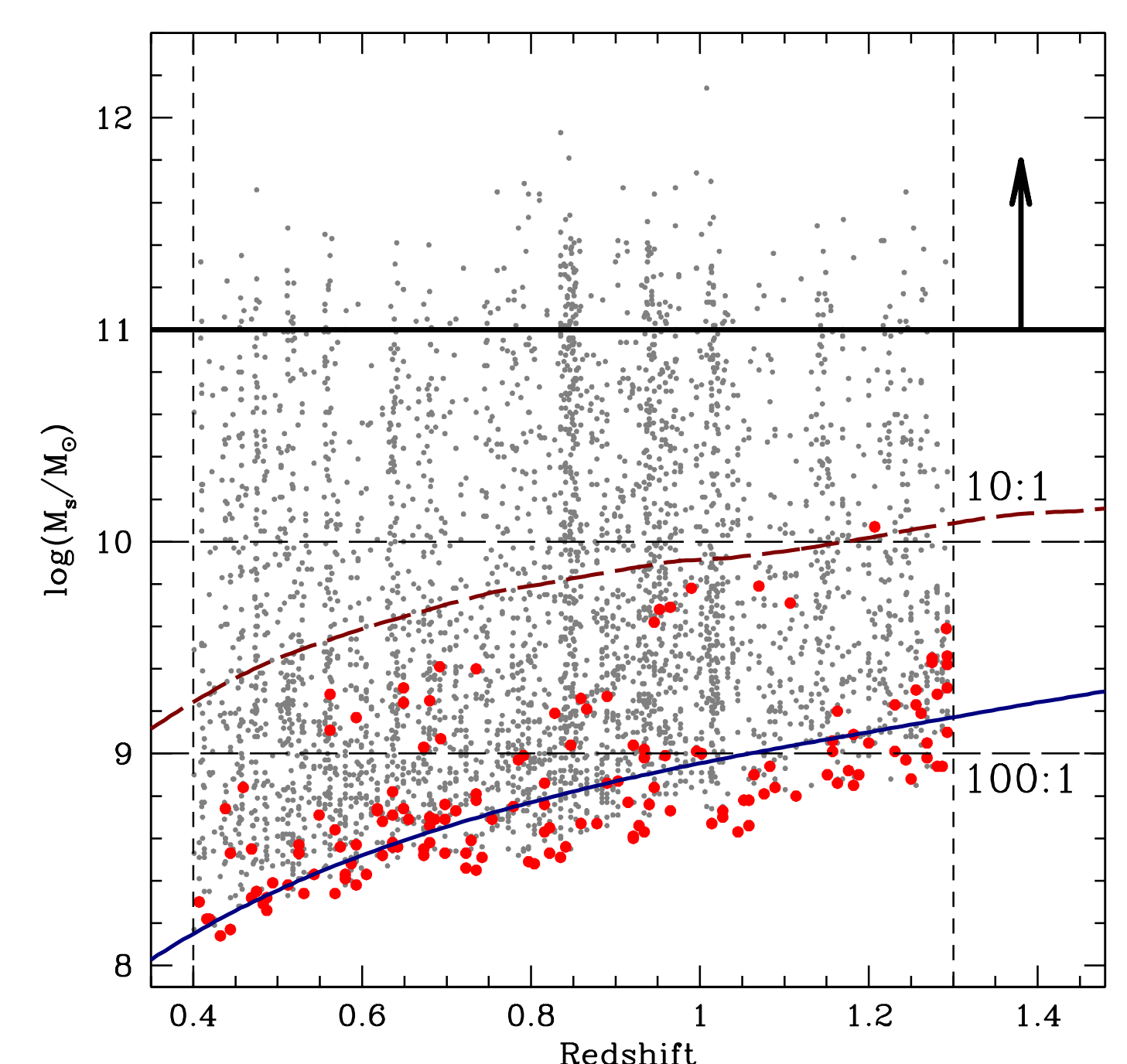


Fig. 1: Redshift vs. stellar mass diagram of SHARDS galaxies. A galaxy is classified as massive if the stellar mass is  $M_s > 10^{11} M_{\odot}$  (arrow and thick horizontal line). The horizontal dashed lines show the limit for 1:10 and 1:100 merger progenitors. The blue solid line shows a  $K_{AB} = 24$  simple stellar population with age 100 Myr, whereas the red dashed line corresponds to a population formed at  $z_{FOR} = 3$  (both at solar metallicity, Chabrier IMF, using the models of [1]).

## 4 AGES OF CENTRAL/SATELLITE PAIRS

Fig. 3 shows the age difference between central and satellite galaxy with respect to the mass ratio. As expected, minor mergers imply a large age difference. Hence, if the bulk of the *second growth phase* proceeds via many minor mergers at a large mass ratio, one would expect a significant spread in the distribution of ages in massive galaxies, producing a noticeable negative radial age gradient, at odds with the observations [4].

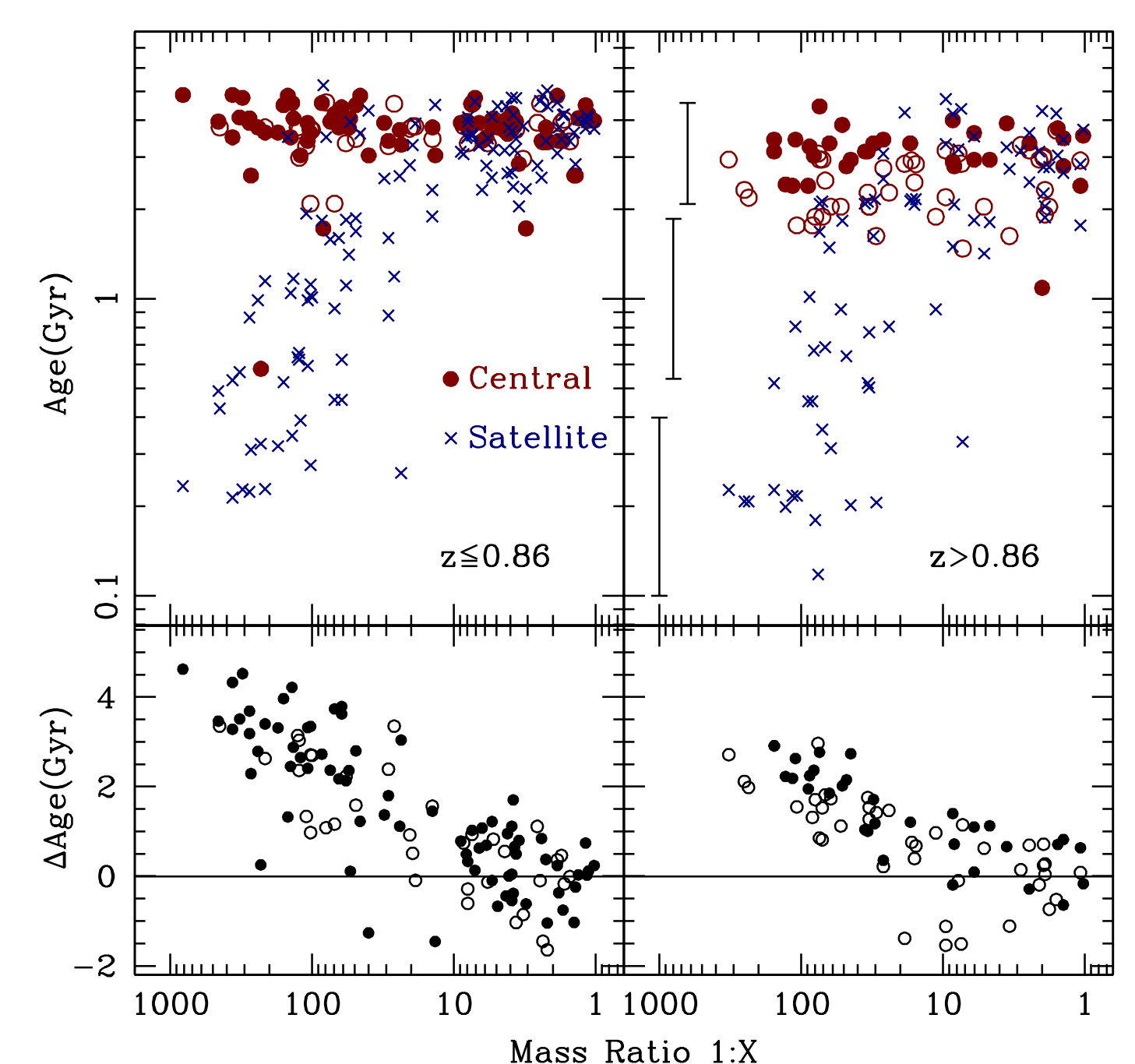


Fig. 3: Age difference of central (red circles: filled for E/S0 or unresolved; open for disc or irregular) and satellite galaxies (blue crosses). The top panels show the individual ages, the bottom panels show the age difference between central and satellite. The sample is split at the median value of the redshift distribution (left/right).

## REFERENCES

- [1] Bruzual, G., Charlot, S., 2003, MNRAS, 344, 1000
- [2] Conselice, C. J., 2006, ApJ, 638, 686
- [3] de la Rosa, I. G., et al. 2011, MNRAS, 418, L74
- [4] La Barbera, F., et al., 2012, MNRAS, 426, 2300
- [5] Marmol-Queralto E., et al., 2012, MNRAS, 422, 2187
- [6] Oser, L., Naab, T., Ostriker, J. P., Johansson, P. H., 2012, ApJ, 744, 63
- [7] Perez-Gonzalez, P. G., et al., 2013, ApJ, 762, 46

# Studying the high-mass end of the mass function at $z \sim 1.7$ in GOODS-S

C. Mancini<sup>\*1</sup>, A. Renzini<sup>1</sup>, E. Daddi<sup>2</sup>

<sup>\*</sup> chiara.mancini@oapd.inaf.it, <sup>1</sup> INAF-OAPD, Padova, (I), <sup>2</sup> Sap-CEA, Saclay (F)

WORK IN PROGRESS

## Abstract

Mass and environment are the main 'drivers' of the quenching of star formation (e.g., Peng et al. 2010,2011). While the environmental effects become stronger at  $z < 1$ , due to the progressive growth of the structures with cosmic epochs, mass-quenching of star formation seems to have a dominant role at higher redshift, i.e., at  $1 < z < 2$ , when the majority of the most massive ( $M^* > 10^{11} M_{\odot}$ ) Early-Type galaxies have formed. Hence, studying the structural and physical properties of the most massive galaxies at  $z \sim 1-2$  can provide crucial insight on the processes that suppressed the star-formation at the earlier epochs. In the recent years, many such studies have been carried out on large samples of galaxies (e.g., Wuys et al. 2011; Newman et al. 2012; Patel et al. 2013, etc.), contributing to improve our knowledge of galaxy evolution using a statistical approach. Instead, in this work we focus on a relatively small sample of galaxies at the high-mass end of the mass-function ( $M^* > 10^{11} M_{\odot}$ ) at redshift  $1.4 < z < 2$  (i.e.,  $z \sim 1.7$ ) in GOODS-S and examine the selected galaxies case by case, so to investigate the morphological differentiation as a function of the specific star-formation rate (sSFR). This has allowed us to unveil peculiar objects that would go unnoticed by a global statistical approach.

## Data, Sample selection and Analysis

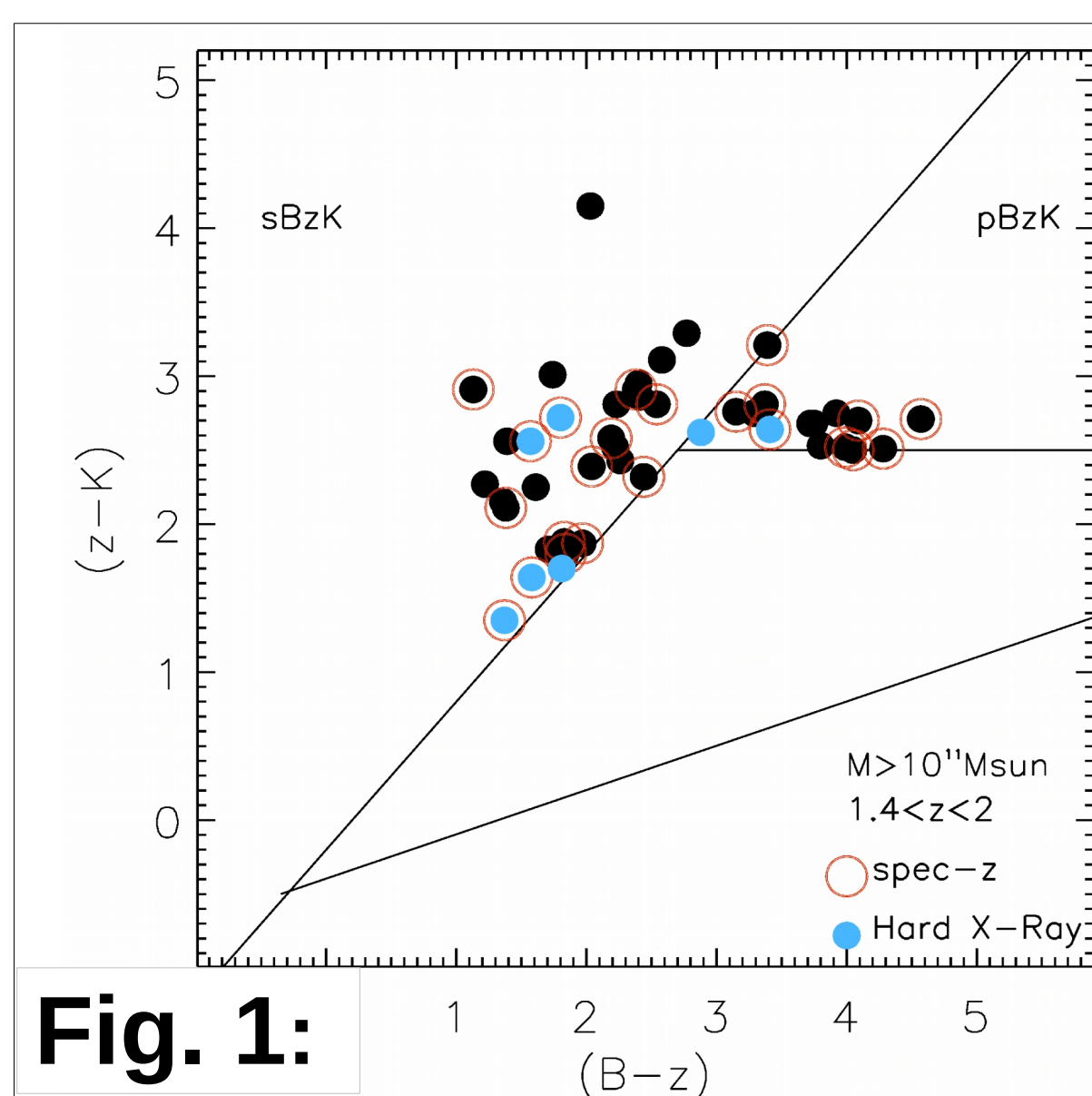


Fig. 1:

A sample of 44 galaxies was culled in GOODS-S starting from the Kvega<22 selected multi-band catalog of Daddi et al. (2007) and applying the following criteria:

- high- $z$  BzK colors (cf., Daddi et al. 2004) (Fig.1)
- $z$ -spec/phot=1.4-2
- Stellar masses  $M^* > 10^{11} M_{\odot}$  (derived from the K-band magnitude, as in Daddi et al. 2004)

The full data-set available in GOODS-S (i.e, HST-CANDELS, Spitzer, Herschel PACS/SPIRE, Chandra/XMM, GMASS/GOODS spectra, etc.) was exploited to characterize the sample galaxies.

Total $M^* > 10^{11} M_{\odot}$	44
Main Sequence	13
Low-sSFR	6
No-MIPS	12
Lense candidates	5
MIPS-blended	8

Table 1. Different sub-categories of objects in our total massive sample

### STAR-FORMATION RATE

The galaxy SFR(IR+UV) was derived from the total LIR obtained by fitting the IR SED (Daddi et al. in prep), and the UV luminosity (L1500) uncorrected for dust extinction, inferred from the  $B$ -magnitude (Kennicutt et al. 1998). For objects undetected in PACS/SPIRE the total LIR was derived from the MIPS/24 $\mu$ m flux according to the empirical relation derived by Elbaz et al. (2011). The Mass-SFR relation for galaxies at  $z \sim 1.7$  (Bethermin et al. 2012) is shown in Fig.2. The sample can be split in three main sub-samples based on the galaxy sSFR (i.e., SFR/ $M^*$ ) as reported in Table 1 :

- 1) Galaxies on the 'Main sequence' (MS) ;
- 2) Galaxies with low sSFR, i.e. more than 4X below the MS (the red line in Fig.2), with sSFR  $< 0.3 \text{ Gy}^{-1}$  ;
- 3) MIPS/24 $\mu$ m undetected galaxies (upper limits in Fig.2).

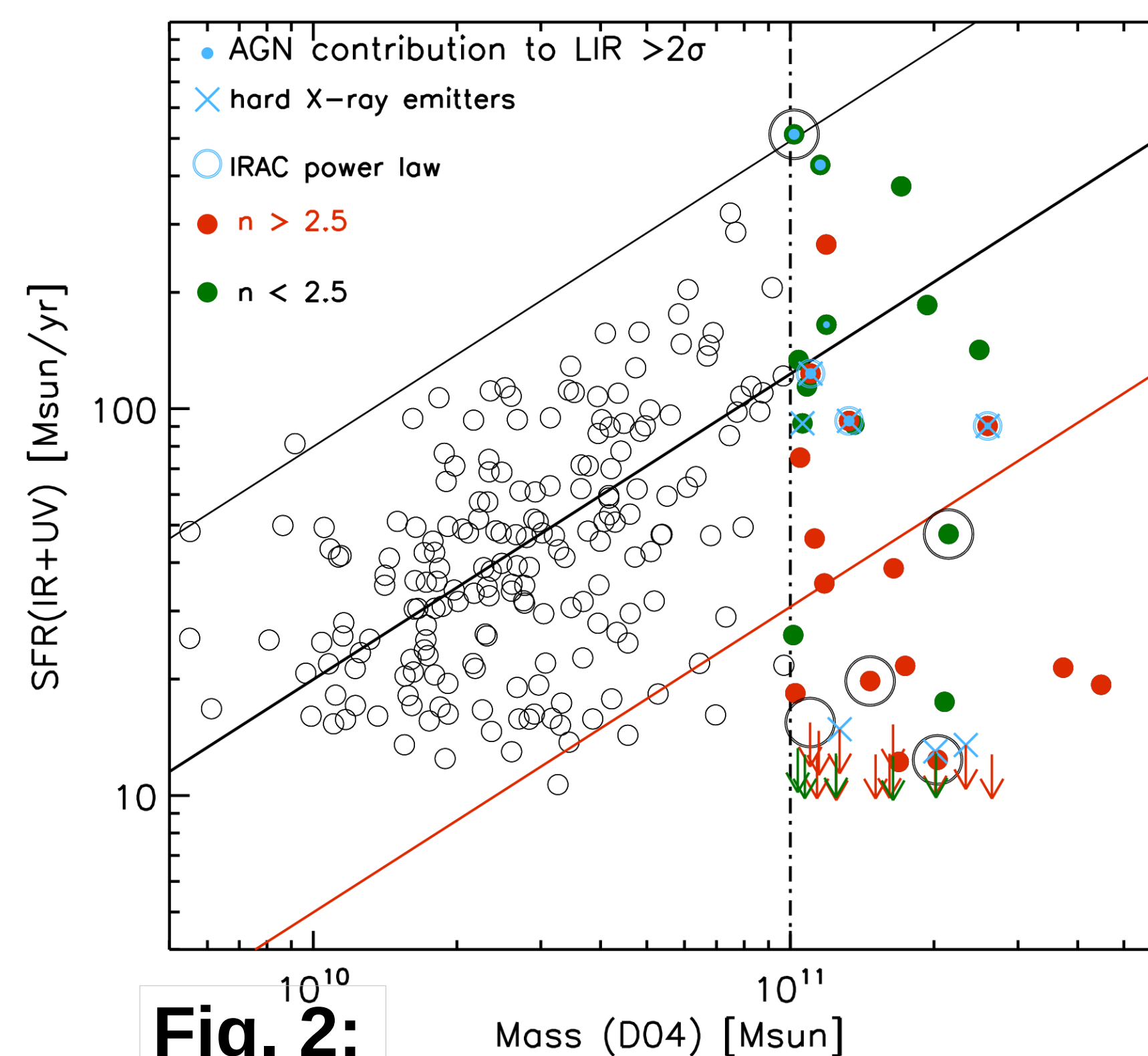


Fig. 2:

### MORPHOLOGY

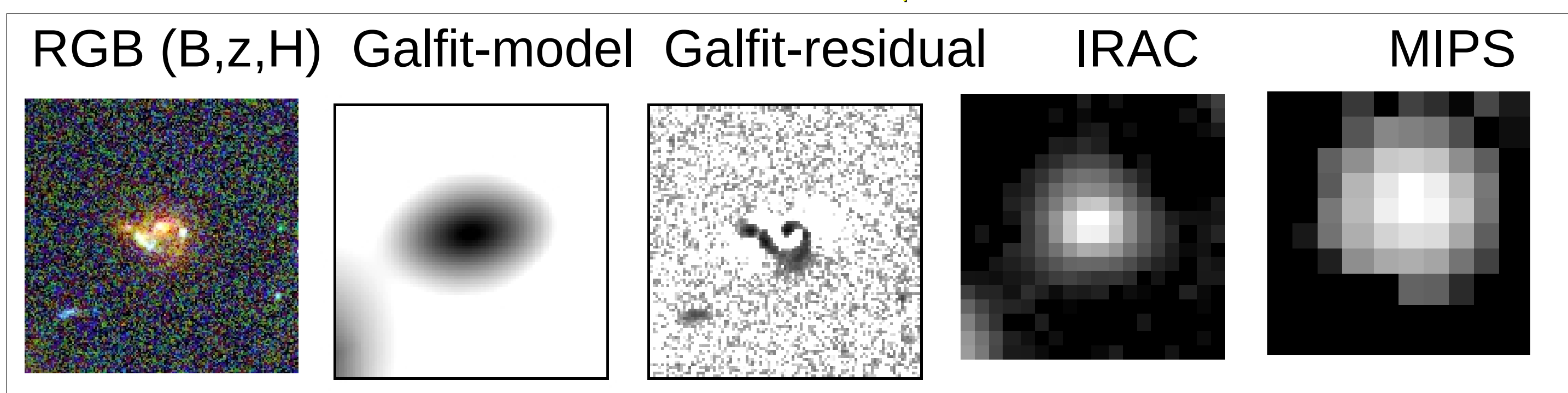
One-component Galfit (Peng et al. 2010) surface-brightness fitting was performed to discriminate between disks (Sersic index,  $n < 2.5$ ) and spheroids ( $n > 2.5$ ) on the Mass-SFR diagram. The results are shown in Fig. 2 and Fig 3.

In Fig. 2 The  $M^* > 10^{11} M_{\odot}$  sample is colour-coded as explained in the legend. It is evident that moving from the top to the bottom part of the high-mass end of the MS the Sérsic index increases indicating a bulge-like structure more and more pronounced, as found by Wuys et al. (2011) and by Salmi et al. (2012) at  $z \sim 1$ .

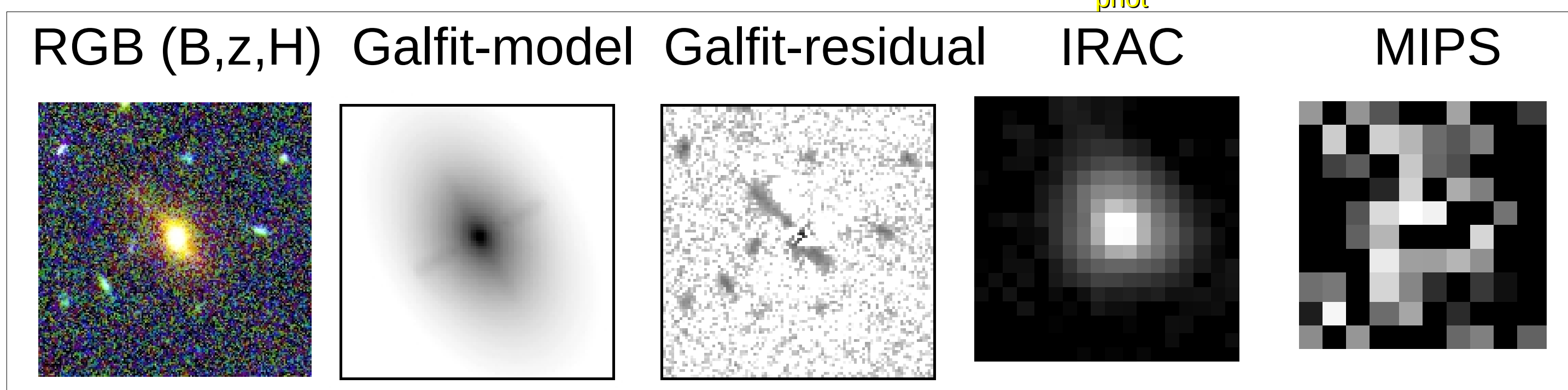
## Morphological differentiation on the MS at $z \sim 1.7$ for $M^* \geq 10^{11} M_{\odot}$

Fig. 3.

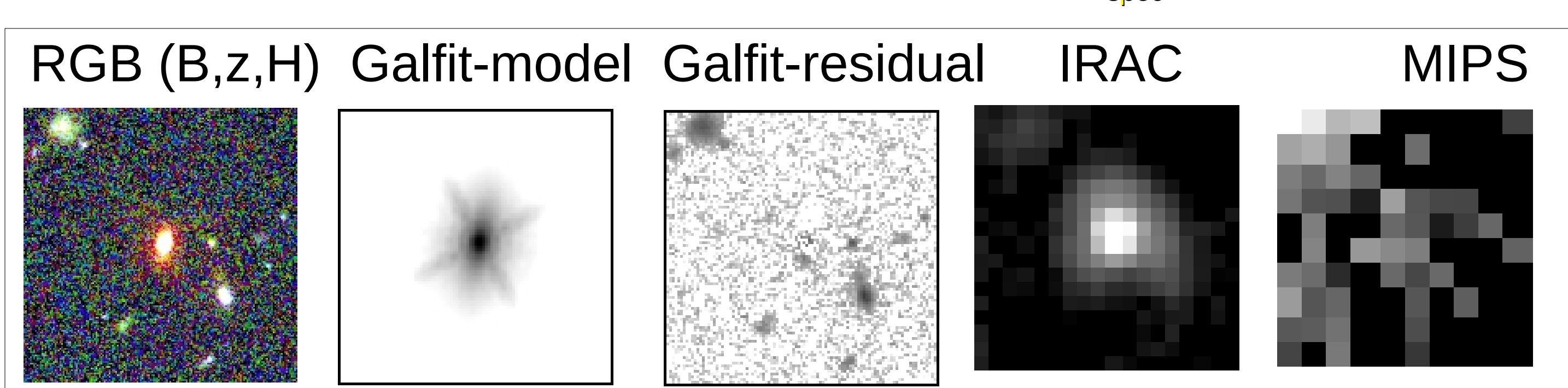
- 1) Main-Sequence sub-sample (#3236,  $z_{\text{spec}} = 1.729$ )



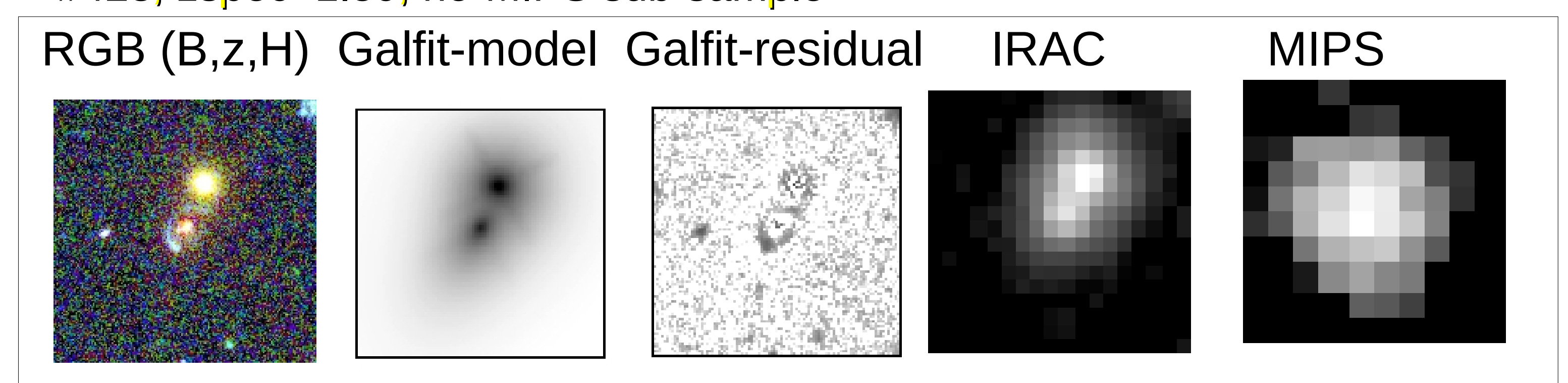
- 2) Low-sSFR sub-sample (SFR < 1/4 x MS) (#856,  $z_{\text{phot}} = 1.76$ )



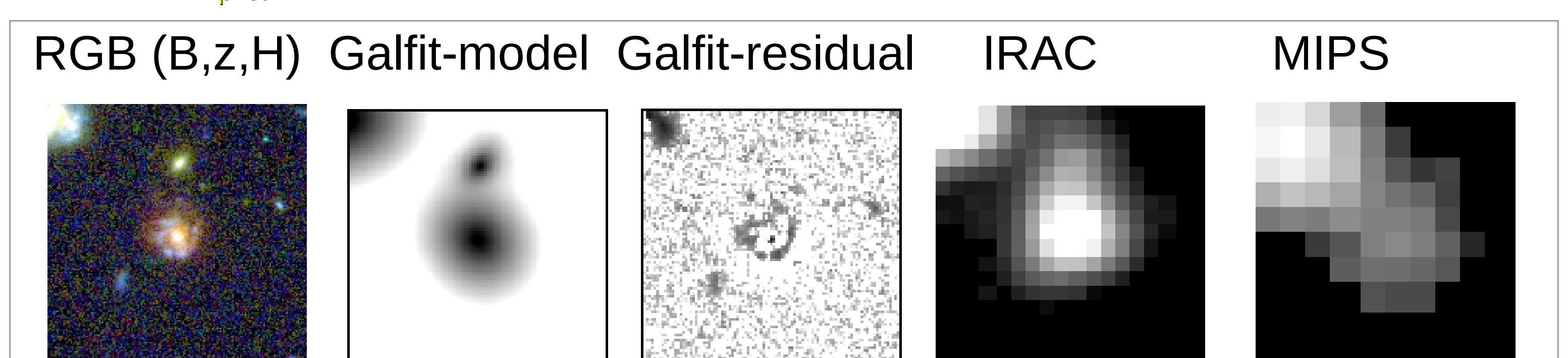
- 3) No-MIPS sub-sample (MIPS/24 $\mu$ m < 3 $\sigma$ ) (#848,  $z_{\text{spec}} = 1.609$ )



In Fig.3, The Left Panels show three galaxies from each of the three different sub-samples on the e Mass-SFR diagram: 1) Main Sequence, 2) Low sSFR, and 3) 24 $\mu$ m undetected galaxies. All the postage stamps are 10 arcsec in size. The sub-sample of 'Low sSFR galaxies' includes many objects with Early-Type morphology, that seems to be in a transient phase between 'Main-Sequence' star-forming galaxies and passive 'no-MIPS' spheroids, such as the object 2) shown in this figure. Our sample also includes a certain number of objects affected by contamination from close neighbours in the mid- and far-IR (i.e., MIPS-blended in Table 1), and also some peculiar objects, such as some lense candidates (highlighted with big black open circles in Fig.2) surrounded by a blue ring (i.e., Bottom Panels, first row). It remains to be established whether some of these objects are instead face-on systems composed by a prominent red bulge and a blue clumpy disk (i.e., the example shown in the Bottom Panels, second row).



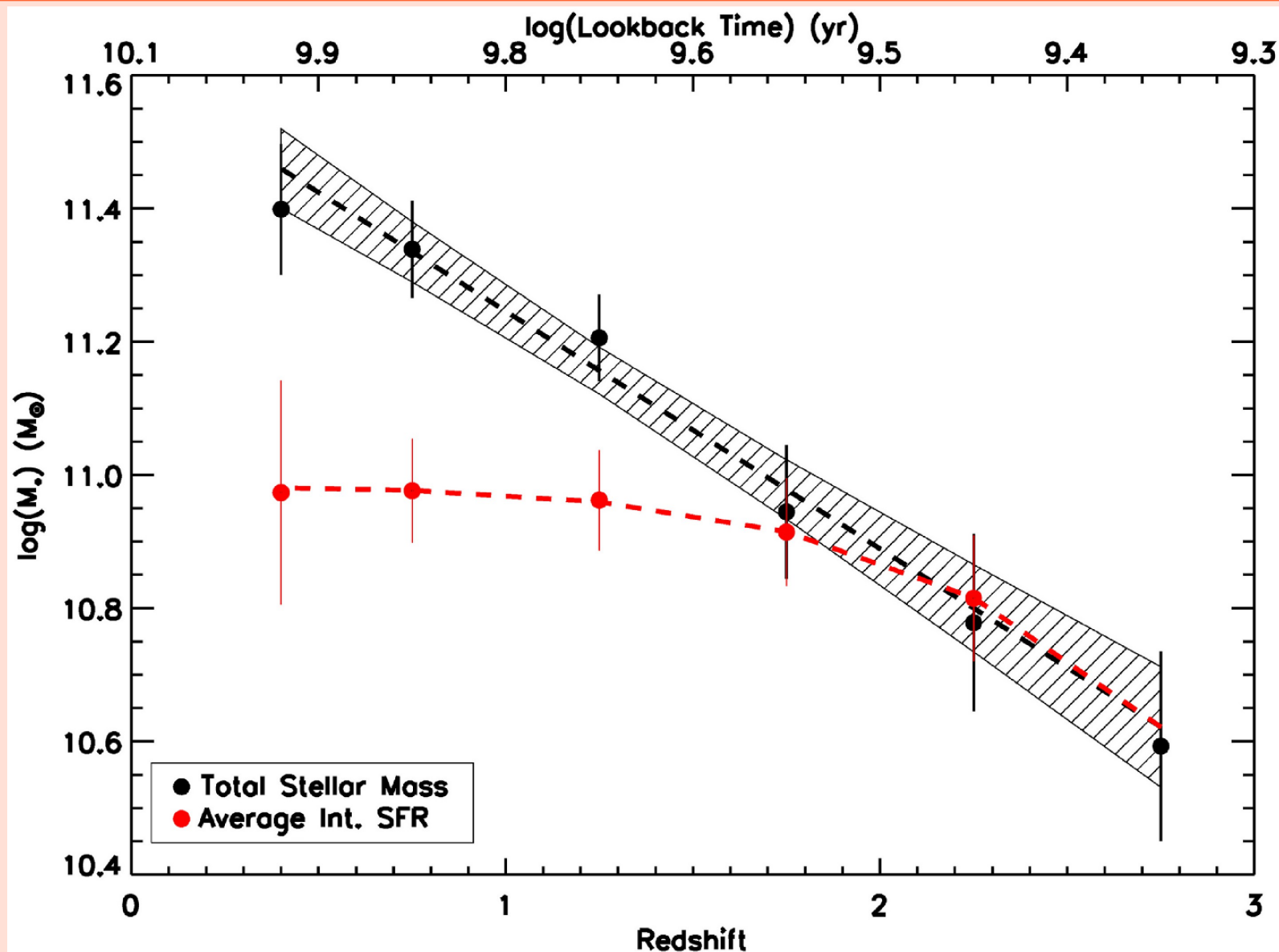
- #8569,  $z_{\text{phot}} = 1.47$ , Low-sSFR sub-sample



# STAR FORMATION VERSUS MINOR MERGERS THE STELLAR MASS GROWTH OF MASSIVE GALAXIES SINCE Z=3

Jamie Ownsworth

ppxjo1@nottingham.ac.uk

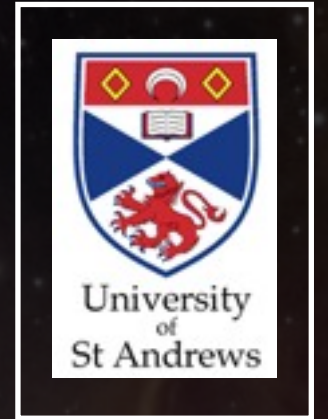


# Following the merger sequence

## Morphological study of the evolution of post-merging galaxies

Milena Pawlik ([mp84@st-andrews.ac.uk](mailto:mp84@st-andrews.ac.uk)),

Vivienne Wild (University of St Andrews), Peter H. Johansson (University of Helsinki), Jakob Walcher (AIP, Potsdam)



## POSTER SUMMARY

- This project's subject are post-mergers - galaxies that appear to have undergone a recent merger;
- The main aim is to develop a method suitable for studying the evolution of post-mergers by quantifying their morphology;
- The first step is to explore literature methods that have been used for galaxy morphology measurements by applying them to samples of post-merger candidates, and to compare the results with outcomes of hydrodynamic simulations;
- Very weak trends in the observational data have been found so far as opposed to stronger trends emerging from the simulations.
- Refinement of the analysis is necessary in order to decide whether these methods are sufficient to study the evolution of post-mergers;
- Ultimately, a new method may be needed, the development of which would then become the long-term goal of this project.



SEDmorph



# Properties of dusty galaxies at high and low redshifts



The University of Nottingham

Kate Rowlands<sup>1</sup>

With: Loretta Dunne, Simon Dye, Alfonso Aragon-Salamanca, Elisabete da Cunha, Dan Smith, Steve Maddox, Haley Gomez + the Herschel ATLAS consortium

Email - [kerowlands@googlemail.com](mailto:kerowlands@googlemail.com)



## Introduction

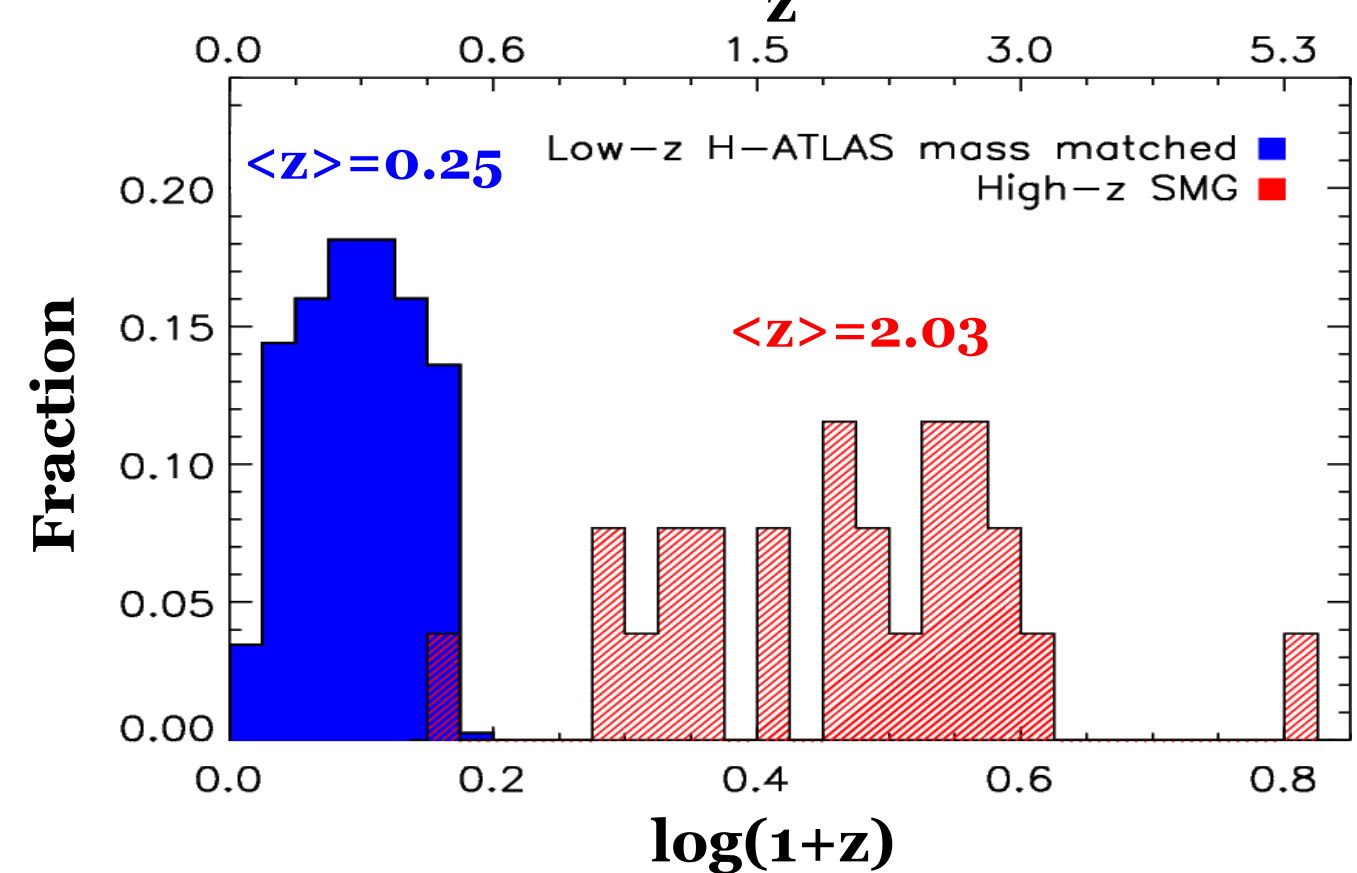
High redshift submillimetre galaxies (SMGs) are the most actively star-forming and dusty galaxies in the Universe. Constraining the properties of these galaxies is important for understanding the evolution of massive galaxies and galaxy evolution models in general. Using panchromatic data from the UV to the submillimetre, we explore the physical properties of a sample of  $\sim 250\mu\text{m}$  rest-frame selected galaxies at high redshift, and compare them to dusty galaxies at low redshift selected in a similar way, to investigate the differences in the dusty galaxy populations over cosmic time.

### Sample $\sim 250\mu\text{m}$ rest-frame selected

#### SMG sample ( $0.48 < z < 5.31$ ) – from Magnelli et al. (2012)

- $850\mu\text{m}$ +PACS/SPIRE ( $100\text{--}500\mu\text{m}$ ) detection.
- Robust multiwavelength counterpart (radio and/or  $24\mu\text{m}$ ).
- Spectroscopic redshift + optical-NIR photometry.

26 galaxies with good SED fits



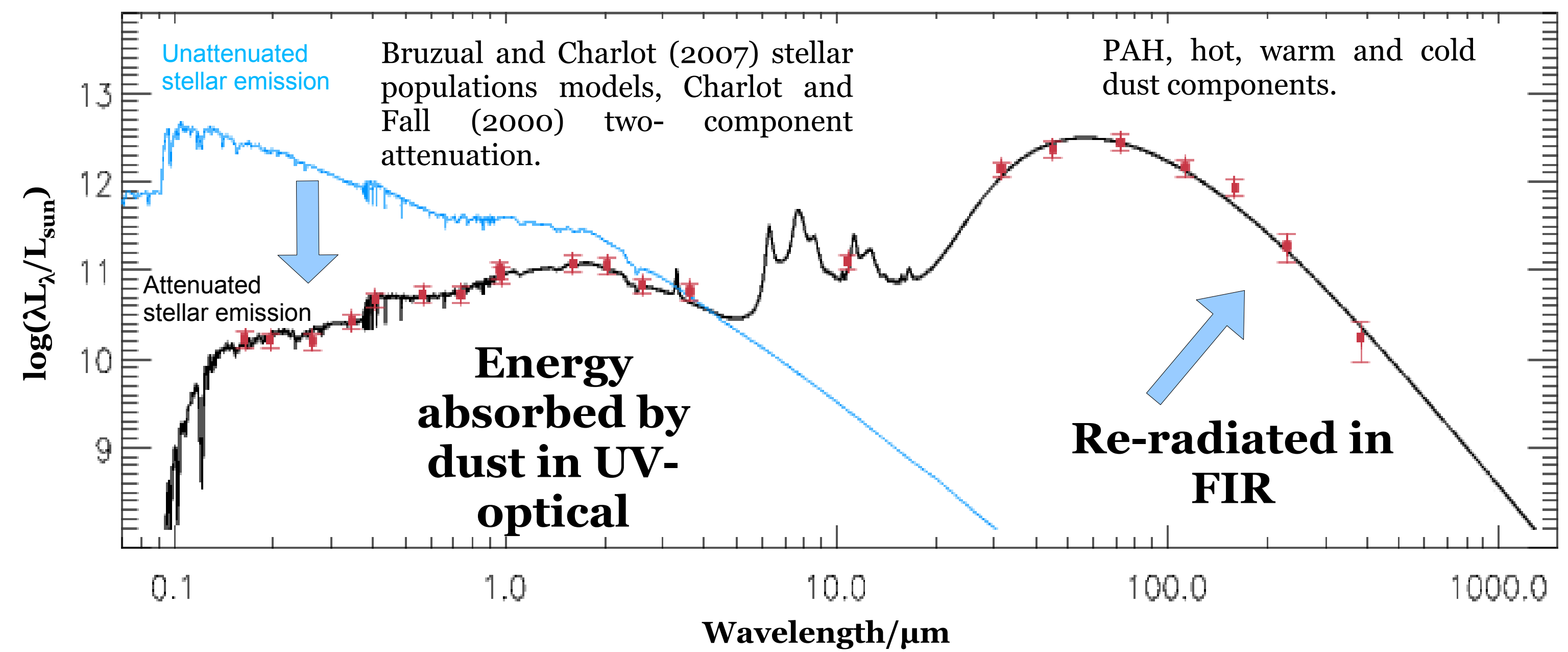
#### H-ATLAS sample ( $0.005 < z < 0.5$ )

- $250\mu\text{m}$   $5\sigma$  detection.
- Reliable optical counterpart (Smith et al. 2011).
- Spectroscopic redshift + GAMA optical photometry (Hill et al. 2011) + good SED fit (Smith et al. 2012)
- Matched in stellar mass to SMG sample.

375 galaxies

### SED fitting - MAGPHYS

- Energy balance model - da Cunha et al. (2008).
- Bayesian approach - statistical constraints on physical parameters:
  - Compare observed galaxy SED to large library of models which encompass all parameter combinations.
  - Build marginalised likelihood distribution of physical parameters - compute  $\chi^2$  goodness of fit for each model - generate probability density function (PDF).



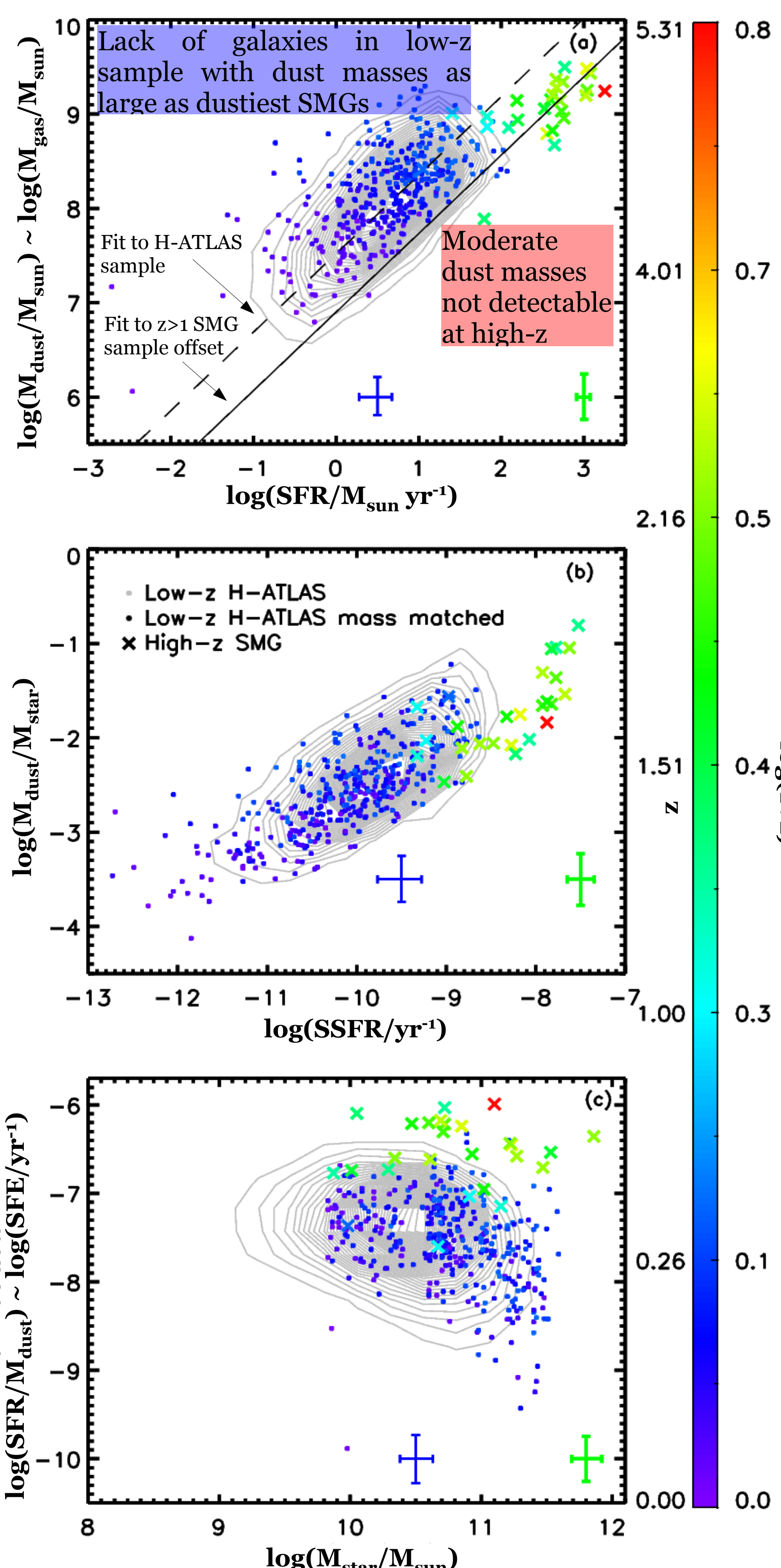
### Properties of $\sim 250\mu\text{m}$ rest-frame selected galaxies

- SMG  $\langle M_{\text{star}} \rangle = 6.0 \times 10^{10} M_{\text{sun}}$ .
- SMG  $\langle \text{SFR} \rangle = 250 M_{\text{sun}}/\text{yr}$ , factor of 80 higher than SFR of low- $z$  H-ATLAS galaxies.
- Lack of highly star-forming galaxies at low- $z$  not a volume effect, H-ATLAS Phase 1 co-moving volume comparable to SMG survey volume ( $1 \times 10^8 \text{ Mpc}^{-3}$ ).
- SMGs have higher  $M_{\text{dust}}$  ( $\langle M_{\text{dust}} \rangle = 1.1 \times 10^9 M_{\text{sun}}$ ) than low- $z$  H-ATLAS galaxies ( $\langle M_{\text{dust}} \rangle = 1.4 \times 10^8 M_{\text{sun}}$ ).
- Larger space density of galaxies with highest dust masses at high- $z$ , galaxies would have been detected in H-ATLAS should they exist at low- $z$ .
- Consistent with **strong evolution in dust content of massive, dusty galaxies with redshift**, in agreement with Dunne and Eales 2001, Dunne et al. 2003, Eales et al. 2010, Dunne et al. 2011, Bourne et al. 2012.

- $M_{\text{dust}} \propto M_{\text{gas}}$ ,  $\rightarrow$  SMGs have higher gas masses than low- $z$  dusty galaxies (assuming constant metallicity).
- **SMGs are offset by 0.6 dex** relative to low- $z$  dusty galaxies  $\rightarrow$  **higher star-formation efficiency**. Consistent with CO studies of SMGs (Greve et al. 2005, Genzel et al. 2010).

- SMGs have  $M_{\text{dust}}/M_{\text{star}}$  consistent with upper end of low- $z$  distribution, but SSFR of SMGs much higher than low- $z$  galaxies.

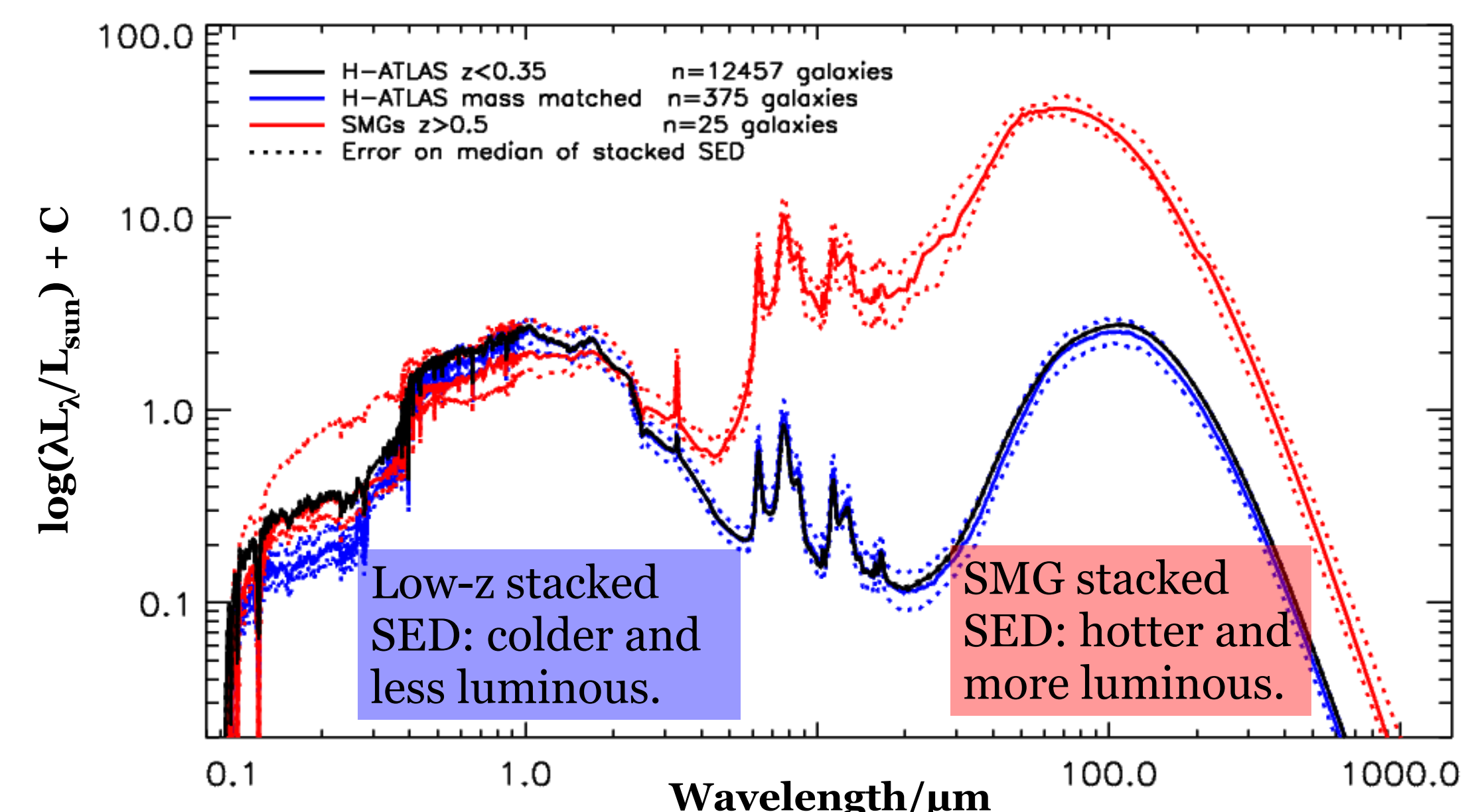
- **SMGs form stars more efficiently** than low- $z$  dusty galaxies of similar stellar mass
  - Mergers?
  - or
  - Dynamical instabilities in high gas fraction disks?



### Stacked SEDs

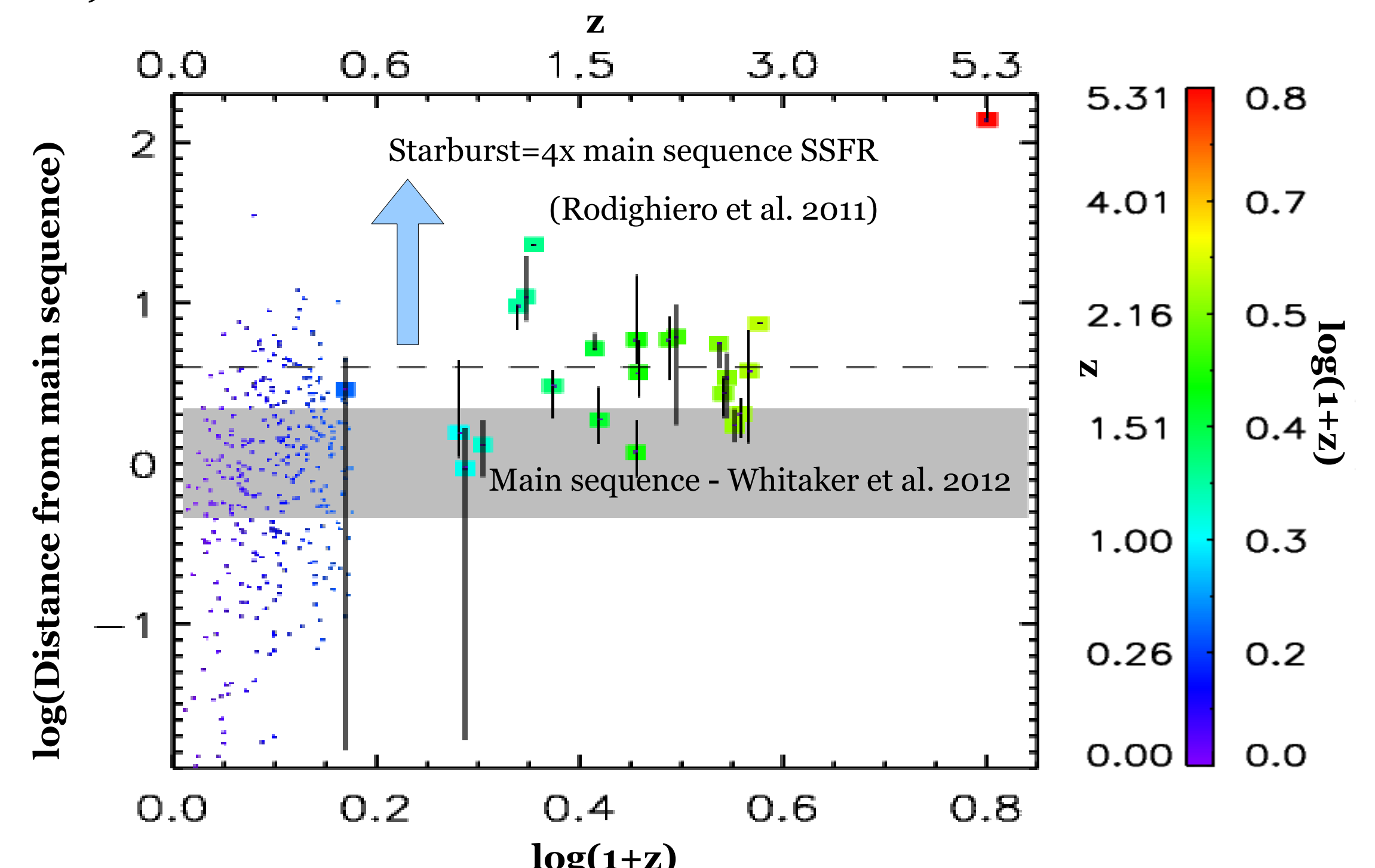
For stacking method see Smith et al. 2012

- Mass matched stacked SED is representative of H-ATLAS sample at  $z < 0.35$ .
- Majority of dust luminosity in SMGs originates from star-forming regions.
- At lower redshifts dust luminosity is dominated by diffuse ISM.



### The nature of star formation in dusty galaxies

- $\sim 7\%$  of low- $z$  galaxies classified as starbursts
- Population of massive, dusty galaxies below the main sequence; these may be shutting down their star formation, but still harbour a substantial amount of dust (Rowlands et al. 2012).
- $\sim 40\%$  of the SMGs lie above main sequence at a given redshift (but be aware selection effects). **SMG population is a mix of massive secularly evolving galaxies and starbursts** (may be merger-driven).



### Conclusions

- SMGs: significantly higher SFRs, dust masses, effective dust temperatures and obscuration than  $z < 0.5$  dusty galaxies selected to have a similar stellar mass. Differences between the high and low- $z$  dusty galaxies may be driven by an increase in gas fraction at high- $z$ .
- Majority of dust luminosity in SMGs originates from star-forming regions, at low- $z$  dust luminosity is dominated by diffuse ISM.
- $\sim 40\%$  of SMGs lie above main sequence of star formation at a given redshift. SMG population is a mix of massive secularly evolving galaxies and starbursts.

- References:
- Bruzual G and Charlot S., 2007, in prep
  - Bourne N., et al. 2012, MNRAS, 421, 3027
  - Charlot S., Fall S. M., 2000, ApJ, 539, 718
  - da Cunha E., Charlot S., Elbaz D., 2008, MNRAS, 388, 1595
  - Dunne L. and Eales S., 2001, MNRAS, 327, 697
  - Dunne L., Eales S., and Edmunds M., 2003, MNRAS, 341, 589
  - Eales S., et al. 2010, A&A, 518, L23
  - Genzel R., et al. 2010, MNRAS, 407, 2091
  - Greve T. R., et al. 2005, MNRAS, 359, 1165
  - Hill D. T., et al., 2011, MNRAS, 412, 765
  - Magnelli et al. 2012, A&A, 538, A155
  - Rodighiero G., et al., 2011, ApJL, 739, L40
  - Rowlands et al. 2012, MNRAS, 419, 2545
  - Smith D. J. B., et al., 2011, MNRAS, 416, 857
  - Smith D. J. B., et al., 2012, MNRAS, 427, 703
  - Whitaker et al. 2012, ApJL, 754, L29